JAMES | Journal of Advances in Modeling Earth Systems®

RESEARCH ARTICLE
10.1029/2025MS004940

Assessing CO_2 Fluxes for European Peatlands in ORCHIDEE-PEAT With Multiple Plant Functional Types

Liyang Liu[1], Chunjing Qiu[2,3], Yi Xi[1], Elodie Salmon[1], Aram Kalhori[4], Rebekka R. E. Artz[5], Christophe Guimbaud[6], Matthias Peichl[7], Joshua L. Ratcliffe[7,8], Koffi Dodji Noumonvi[7], Efrén López-Blanco[9,10], Jiří Dušek[11], Tiina Markkanen[12], Torsten Sachs[4,13], Mika Aurela[12], Thu-Hang Nguyen[1], Annalea Lohila[12], Ivan Mammarella[14], and Philippe Ciais[1]

[1]Laboratoire des Sciences du Climat et de l'Environnement, LSCE/IPSL, CEA–CNRS–UVSQ, Université Paris-Saclay, Gif-sur-Yvette, France, [2]Research Center for Global Change and Complex Ecosystems, School of Ecological and Environmental Sciences, East China Normal University, Shanghai, China, [3]Institute of Eco-Chongming, East China Normal University, Shanghai, China, [4]GFZ Helmholtz Centre for Geosciences, Potsdam, Germany, [5]The James Hutton Institute, Aberdeen, UK, [6]Laboratoire de Physique et de Chimie de l'Environnement et de l'Espace, LPC2E, CNRS, OSUC, University Orleans, Orleans, France, [7]Department of Forest Ecology and Management, Swedish University of Agricultural Sciences, Umeå, Sweden, [8]Unit for Field-Based Forest Research, Swedish University of Agricultural Sciences, Vindeln, Sweden, [9]Department of Ecoscience, Arctic Research Center, Aarhus University, Frederiksborgvej, Roskilde, Denmark, [10]Department of Environment and Minerals, Greenland Institute of Natural Resources, Nuuk, Greenland, [11]Global Change Research Institute of the Czech Academy of Sciences, Brno, Czech Republic, [12]Climate System Research, Finnish Meteorological Institute, Helsinki, Finland, [13]Institute of Geoecology, Technische Universität Braunschweig, Braunschweig, Germany, [14]Faculty of Science, Institute for Atmospheric and Earth System Research/Physics, University of Helsinki, Helsinki, Finland

Key Points:

- A new version of the ORCHIDEE-PEAT model (v.3.0) with 4 peatland-specific plant functional types (graminoid, shrub, moss and lichen, and tree) was developed
- Ten key parameters controlling photosynthesis, autotrophic respiration, and soil carbon decomposition have been calibrated
- The performance of modeled CO_2 fluxes has been evaluated against eddy-covariance (EC) observations from 14 European peatland sites

Supporting Information:

Supporting Information may be found in the online version of this article.

Correspondence to:

C. Qiu,
cjqiu@des.ecnu.edu.cn

Citation:

Liu, L., Qiu, C., Xi, Y., Salmon, E., Kalhori, A., Artz, R. R. E., et al. (2025). Assessing CO_2 fluxes for European peatlands in ORCHIDEE-PEAT with multiple plant functional types. *Journal of Advances in Modeling Earth Systems*, *17*, e2025MS004940. https://doi.org/10.1029/2025MS004940

Received 21 JAN 2025
Accepted 23 MAY 2025

Author Contributions:

Conceptualization: Chunjing Qiu, Philippe Ciais
Data curation: Liyang Liu, Elodie Salmon, Aram Kalhori, Rebekka R. E. Artz, Christophe Guimbaud, Matthias Peichl, Joshua L. Ratcliffe, Koffi Dodji Noumonvi, Efrén López-Blanco, Jiří Dušek, Tiina Markkanen, Torsten Sachs, Mika Aurela, Annalea Lohila, Ivan Mammarella
Formal analysis: Liyang Liu, Thu-Hang Nguyen

Abstract

Peatlands are significant carbon reservoirs vulnerable to climate change and land use change such as drainage for cultivation or forestry. We modified the ORCHIDEE-PEAT global land surface model, which has a detailed description of peat processes, by incorporating three new peatland-specific plant functional types (PFTs), namely deciduous broadleaf shrub, moss and lichen, as well as evergreen needleleaf tree in addition to previously peatland graminoid PFT to simulate peatland vegetation dynamic and soil CO_2 fluxes. Model parameters controlling photosynthesis, autotrophic respiration, and carbon decomposition have been optimized using eddy-covariance observations from 14 European peatlands and a Bayesian optimization approach. Optimization was conducted for each individual site (single-site calibration) or all sites simultaneously (multi-site calibration). Single-site calibration performed better, particularly for gross primary production (GPP), with root mean square deviation (RMSD) reduced by 53%. While multi-site calibration showed limited improvement (e.g., RMSD of GPP reduced by 22%) due to the model's inability to account for spatial parameter variations under different climatic contexts (trait-climate correlations). Site-optimized parameters, such as $\mathbf{Q_{10}}$, the temperature sensitivity of heterotrophic respiration, revealed strong empirical relationships with environmental factors, such as air temperature. For instance, $\mathbf{Q_{10}}$ decreased significantly at warmer sites, consistent with independent field data. To improve the model by using the lessons from single-site optimization, we incorporated two key trait-climate relationships for $\mathbf{Q_{10}}$ and $\boldsymbol{V}_{\mathbf{cmax}}$ (maximum carboxylation rate) into a new version of the ORCHIDEE-PEAT models. Using this description of spatial variability of parameters holds significant promise for improving the accuracy of carbon cycle simulations in peatlands.

Plain Language Summary

Peatlands store substantial amounts of carbon and are vulnerable to climate change. To better simulate how peatlands behave, we developed a new version of a computer model called ORCHIDEE-PEAT, in which three new types of plants that are specific to peatlands: deciduous broadleaf shrubs, mosses and lichens, as well as evergreen needle leaf trees were added in addition to previously peatland graminoids. The model has been used to simulate the CO_2 fluxes (gross primary production and net ecosystem CO_2 exchange) of 14 European peatlands. Several important parameters of the model were calibrated for each individual site (single-site calibration) and all sites together (multi-site calibration). The model using single-site calibrated parameters exhibited good performance, especially for plant photosynthesis. Furthermore, we found that the values of calibrated parameters, or traits, varied along with different climate conditions (i.e., air temperature). Without accounting for this variation of model parameters, modeled photosynthesis and net ecosystem exchange of CO_2 using a single set of parameters for all sites (multi-site calibration) only slightly

Funding acquisition: Philippe Ciais
Methodology: Liyang Liu, Chunjing Qiu, Yi Xi, Philippe Ciais
Project administration: Philippe Ciais
Software: Liyang Liu, Yi Xi
Supervision: Chunjing Qiu, Philippe Ciais
Writing – original draft: Liyang Liu
Writing – review & editing: Liyang Liu, Chunjing Qiu, Yi Xi, Elodie Salmon, Aram Kalhori, Rebekka R. E. Artz, Christophe Guimbaud, Matthias Peichl, Joshua L. Ratcliffe, Koffi Dodji Noumonvi, Efrén López-Blanco, Jiří Dušek, Tiina Markkanen, Torsten Sachs, Mika Aurela, Thu-Hang Nguyen, Annalea Lohila, Ivan Mammarella, Philippe Ciais

improved the model performance compared with default simulations. Incorporating the effect of climate on model parameters, that is trait-climate correlations, in future model development is necessary to improve model performance.

1. Introduction

The northern peatlands, spanning an area of 3.5–4.0 million km^2 (Gorham, 1991; Turunen et al., 2002; Yu et al., 2010), occupy 2%–3% of the terrestrial land area and represent a large mass of soil organic carbon (SOC) ranging from 270 to 540 Pg C (1 Pg = 10^{15}g) (Frolking & Roulet, 2007; Parish et al., 2008; Yu, 2012). The carbon mass of northern peatland accounts for about one-sixth of the global total SOC, while there is large uncertainty in the global total SOC with estimates ranging from 504 to 3,000 Pg C (Scharlemann et al., 2014). Peatlands represent a long-term sink of carbon dioxide (CO_2) and a source of methane (CH_4) (Frolking et al., 2011; Treat et al., 2019), hence playing an important role in regulating the global climate and global greenhouse gas (GHG) balance (MacDonald et al., 2006; Mikaloff Fletcher et al., 2004; Smith et al., 2004). Under natural conditions, peatlands are carbon sinks with an estimated accumulation rate between 0.5 and 1 mm per year since their formation (Minasny et al., 2019). However, human disturbance and climate change are switching some peatlands from net sink to the net source of carbon (Leifeld et al., 2019; Leifeld & Menichetti, 2018; Turetsky et al., 2002). Leifeld et al. (2019) estimated that global peatlands turned from a net sink to a net source of GHGs around the 1960s, due to extensive drainage and land use conversion, particularly in Europe. Moreover, the combined effects of anthropogenic activities and climate change-driven changes, such as temperature and precipitation, make the fate of the large global peatland C stock highly uncertain (Artz et al., 2022; Loisel et al., 2021; Qiu et al., 2021).

Few land surface models (LSMs) for example, LPJ-GUESS (Chaudhary et al., 2017), PTEM (Zhao et al., 2022) and HPM (Frolking et al., 2010), incorporated representations of the biogeochemical and physical processes of peatlands, encompassing the exchange of energy and various substances such as water, carbon, and nitrogen (Mozafari et al., 2023). Some of these LSMs introduced peatland-specific plant functional types (PFTs). For those who employ a unique peatland PFT in the model, the peatland vegetation is treated as C3 graminoids (Chadburn et al., 2022; Qiu et al., 2018, 2019). While for those who employ multiple peatland PFTs to account for complex vegetation composition found in peatlands, typically they include graminoids (i.e., grasses, sedges and herbaceous plants) and mosses/lichens (Spahni et al., 2013; Wania et al., 2009a, 2009b), and very few consider (dwarf) shrubs (Zhao et al., 2022; Chaudhary et al., 2017; Frolking et al., 2010) and trees (Bona et al., 2020; St-Hilaire et al., 2010; Zhang et al., 2002). The number of PFTs considered in models plays an important role in explaining carbon and energy fluxes because variations in functional traits across different PFTs lead to distinct responses to environmental conditions (Dorrepaal, 2007; Kuiper et al., 2014; Laine et al., 2022). It is increasingly recognized that alterations in vegetation composition significantly impact peatland carbon cycling, and their feedbacks on future climate change (Robroek et al., 2015, 2016; Walker et al., 2015). Consequently, it is important to improve the representation of peatland vegetation diversity using the PFT composition in LSMs.

The peatland-specific version of the Organizing Carbon and Hydrology In Dynamic Ecosystems (ORCHIDEE) LSM, known as ORCHIDEE-PEAT (Qiu et al., 2018, 2019), has been developed to simulate the hydrology, energy, and carbon cycles of sphagnum dominated peatlands. It has been applied to investigate the responses of northern peatlands to future climate change (Qiu et al., 2020) and conversion to cropland after drainage (Qiu et al., 2021). Nevertheless, the previous versions of ORCHIDEE-PEAT only employed a graminoid PFT based on C3 grass (Krinner et al., 2005), in which the productivity and rooting depth were reduced, to represent peatland vegetation (Qiu et al., 2018). Recognizing the need for a more nuanced representation of peatland vegetation, this study introduces a novel iteration, labeled as ORCHIDEE-PEAT v.3.0. This updated version incorporates three additional peatland-specific PFTs, they are shrub, moss and lichen, as well as tree, providing a more dynamic representation of peatland vegetation composition. It will enhance the quantification of peatland feedback to climate change and the accuracy of the global projections concerning the effects of peatland vegetation changes on the carbon cycle.

2. Methods

2.1. Model Description

ORCHIDEE-PEAT (Qiu et al., 2018, 2019) is a specifically developed version of ORCHIDEE-MICT to simulate northern peatland dynamics. As a branch of the ORCHIDEE LSM, ORCHIDEE-MICT features an improved representation of high-latitude processes (Guimberteau et al., 2018). An independent hydrological soil tile (different from tiles with upland grasses and trees) was introduced in the ORCHIDEE-PEAT model to represent peatland, incorporating peat-specific soil hydrology. This tile receives surface runoff from other non-peatland soil tiles while maintaining zero bottom drainage flux, and has an additional above-surface water reservoir that can fill up with rainfall and added runoff (Booth et al., 2005; Largeron et al., 2017). Moreover, a set of peat-specific hydraulic parameters, such as large porosity (0.9 m^3 m^{-3}) and high saturated water conductivity (2,120 mm d^{-1}), are used based on field measurements of peat hydraulics (Dawson, 2006; Letts et al., 2000; Wania et al., 2009a; Wu et al., 2016), which enhance water percolation, storage, and retention in peat soil (Qiu et al., 2018, 2019). Peatland vegetation is represented by a C3 graminoid PFT, which integrates sedges, grasses and herbaceous plants. Peat-carbon decomposition is controlled by soil temperature and moisture conditions. The model has been tested at both site (v.1.0, Qiu et al., 2018) and regional (v.2.0, Qiu et al., 2019) scales.

Druel et al. (2017) added non-vascular plants (mosses and lichens), arctic shrubs and arctic C3 grasses into the ORCHIDEE model (ORC-HL-VEG v1.0) to enable a more detailed representation of high-latitude vegetation, and analyzed the impact of including these new PFTs on the net and gross carbon fluxes and the surface energy budgets over the boreal and arctic zone. In this study, to improve the representation of peatland vegetation, the mosses and lichens, and shrubs parameterizations developed by Druel et al. (2017) are adapted and incorporated into the ORCHIDEE-PEAT model. In addition, one of the sites is dominated by trees (FI-Let, Section 2.3), and for parameterizing the peat tree PFT at this site, the same equations as the boreal needleleaf evergreen tree PFT (Krinner et al., 2005) are used, though the parameters of this new tree PFT of peatland are not optimized in this study. In summary, the latest version (v.3.0) of ORCHIDEE-PEAT developed in this study includes four peatland-specific PFTs: they are graminoid, deciduous broadleaf shrub, moss and lichen, as well as evergreen needleleaf tree.

Shrubs share similar biogeochemical and biophysical processes to trees, but grow faster and therefore colonize landscapes before trees. For the northern high latitudes, a new peatland shrub PFT is parameterized using the same equations as the boreal deciduous broadleaf tree PFT (Krinner et al., 2005), but with a lower residence time of C in living tissues and a higher fraction of gross primary production (GPP) lost as growth respiration (Druel et al., 2017).

As described in Druel et al. (2017), Mosses and lichens have no wood and root, with the biomass of mosses and lichens being represented by a leaf pool (95%) and a fruit pool (5%). Vascular plants have stomata that regulate gas fluxes (Ruszala et al., 2011). For non-vascular plants like mosses, the situation is more complex and diverse (Chater et al., 2013; Williams & Flanagan, 1996): some species, such as *Oedipodium*, have “non-active” stomata (Ruszala et al., 2011); others, like *Sphagnum*, have only “pseudo-stomata”; and some, such as *Andreaeobryum*, lack stomata entirely (Haig, 2013). For simplicity and due to the lack of a well-established photosynthesis model for non-vascular plants, mosses and lichens were assumed to have “pseudo-stomata” (Yin & Struik, 2009). In addition, most species of non-vascular plants have been reported to be C3 plants (Aro & Gerbaud, 1984; Bruhl & Wilson, 2007; Teeri, 1981; Toet et al., 2006). Therefore, the equation used to calculate the stomatal conductance of C3 plants, based on Farquhar et al. (1980), has been adopted. However, the values of parameters were adjusted to reduce the dependence of stomatal conductance on vapor pressure deficit (VPD) (Text S1 in Supporting Information S1). Mosses and lichens also have good resistance in cold conditions (Turetsky et al., 2012), which is considered in the model by prolonging their leaf senescence (Druel et al., 2017). Specifically, the leaf senescence parameter is 470 days for mosses and lichens (in contrast to 120 days for C3 grass). However, this adaptation comes with a biomass cost which is modeled through an additional carbon loss based on the cumulative number of days when Net Primary Productivity is negative or zero (Equation 3 in Druel et al., 2017). During the growing season, the leaf turnover rate is increased if the leaf area index (LAI) reaches a certain threshold value, because a thicker moss layer with a higher LAI reduces light penetration to underlying layers (Equation 4 in Druel et al., 2017). To keep an internal coherence between PFTs and treat the competition for water between PFTs in the model, mosses and lichens are assumed to only have access to water in the topsoil (about 0.98 mm) through their leaf-like structures (phyllids). However, the water content decreases significantly during and after the water stress

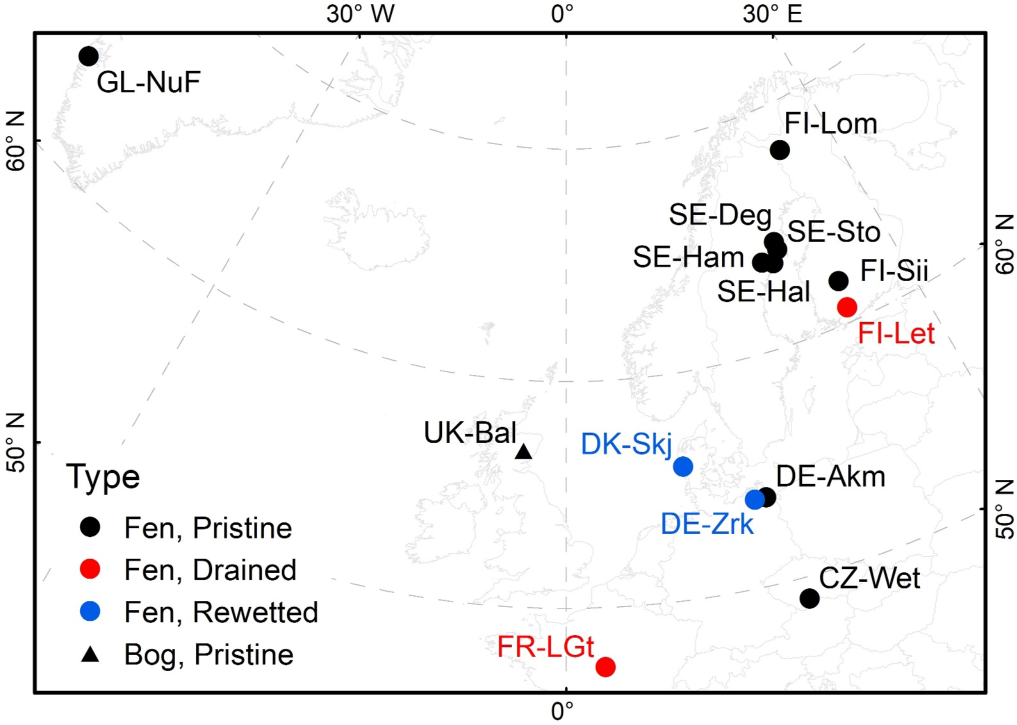

Figure 1. The distribution of 14 sites used in this study. Circles and triangles represent fen and bog, respectively. The dark, red, and blue marks indicate pristine, drained, and rewetted peatlands, respectively.

period, thus the photosynthetic capacity will be reduced (Dimitrov et al., 2011; Wania et al., 2009b; Williams & Flanagan, 1996). To consider this mechanism, a desiccation factor was employed to scale the maximum rate of carboxylation ($V_{\mathbf{cmax}}$) as well as the maintenance respiration (Druel et al., 2017).

The moss and lichen PFT and shrub PFT added by Druel et al. (2017) were not specifically parameterized for peatlands, and significant modifications have been implemented in the model since the publication of ORCHIDEE-PEAT version (Guimberteau et al., 2018; Qiu et al., 2018, 2019). Therefore, it is crucial to optimize and evaluate the model using in situ observations from peatlands to ensure an accurate representation of peatland vegetation and C dynamics.

2.2. Site Description and Simulation Setup

We assessed the performance of ORCHIDEE-PEAT v.3.0 in simulating CO_2 fluxes at 14 European peatland sites, including 13 fens and 1 bog (Figure 1 and Table 1). These sites spread from temperate to arctic regions, with their latitudes ranging from 47.32° to 68.00°N. The long-term (1981–2020) mean annual temperature (MAT) and mean annual precipitation, range from −1.3°C to 12.1°C and 504.6–1346.5 mm, respectively (Table 1). Of these sites, 10 are pristine, two are rewetted (DK-Skj, DE-Zrk), and two are drained peatlands (FI-Let, FR-LGt). The vegetation composition varies across sites. For instance, one site (FI-Let) is covered by trees. Among the seven sites dominated by graminoids, two sites are entirely covered by graminoids (DE-Zrk and DK-Skj), two sites are covered by a mixture of graminoids and shrubs (CZ-Wet and DE-Akm), and the vegetation at the other three sites consist of mixtures of graminoids, mosses and lichens and/or shrubs. Six sites are primarily covered by mosses and lichens, followed by graminoids. Shrubs have relatively low coverage except at the DE-Akm site. The relative area fraction of each site was estimated based on field measurements or literature and fixed constant in the model. More details about the vegetation cover at each site can be found in Text S2 in Supporting Information S1.

Quality-controlled half-hourly or hourly CO_2 fluxes observations including GPP and net ecosystem CO_2 exchange (NEE), with GPP partitioned by using the nighttime approach (NT, Reichstein et al., 2005), and meteorological forcing data including air temperature, wind speed, wind direction, longwave incoming radiation, shortwave incoming radiation, specific humidity, atmospheric pressure, and precipitation were provided by site

Table 1
Site Characteristics of the 14 Peatlands Across Europe

									PFT fractions				
Sites	Lat	Lon	Climatic zone	Type	Period	WTD	MAT (°C)	MAP (mm)	*G*[a]	*S*	*M*	*T*	Reference
CZ-Wet	49.02	14.77	Temperate	fen, pristine	2020–2021	Y	8.6	599.1	0.8	0.2	0.0	0.0	Mejdová et al. (2021)
DE-Akm	53.87	13.68	Temperate	fen, pristine	2010–2014	N	9.1	578.8	0.5	0.5	0.0	0.0	Bernhofer et al. (2016)
DE-Zrk	53.88	12.89	Temperate	fen, rewetted	2014–2017	Y	9.3	606.8	1	0.0	0.0	0.0	Kalhori et al. (2024)
DK-Skj	55.91	8.40	Temperate	fen, rewetted	2020–2021	N	9.0	837.5	1	0.0	0.0	0.0	Herbst et al. (2011)
FI-Let	60.64	23.96	Temperate	fen, drained	2010–2015	Y	4.9	649.7	0.2	0.05	0.25	0.5	Leppä et al. (2020)
FI-Lom	68.00	24.21	Boreal	fen, pristine	2007–2019	Y	−0.8	504.6	0.33	0.1	0.57	0.0	Aurela et al. (2015)
FI-Sii	61.83	24.19	Boreal	fen, pristine	2018–2021	Y	4.1	612.4	0.26	0.1	0.64	0.0	Aurela et al. (2007)
FR-LGt	47.32	2.28	Temperate	fen, drained	2017–2021	N	12.1	676.1	0.3	0.3	0.4	0.0	D'Angelo et al. (2021)
GL-NuF	64.13	−51.39	Boreal	fen, pristine	2008–2016	N	−1.3	1088.6	0.5	0.2	0.3	0.0	López-Blanco et al. (2017)
SE-Deg	64.18	19.56	Boreal	fen, pristine	2014–2022	Y	2.1	640.3	0.44	0.11	0.45	0.0	Noumonvi et al. (2023)
SE-Hal	64.16	19.55	Boreal	fen, pristine	2020–2022	Y	2.1	640.3	0.5	0.07	0.43	0.0	Noumonvi et al. (2023)
SE-Ham	64.16	19.57	Boreal	fen, pristine	2020–2022	Y	2.1	640.3	0.36	0.21	0.43	0.0	Noumonvi et al. (2023)
SE-Sto	64.17	19.56	Boreal	fen, pristine	2020–2022	Y	2.1	640.3	0.37	0.15	0.48	0.0	Noumonvi et al. (2023)
UK-Bal[b]	56.92	−3.16	Temperate	bog, pristine	2018–2020	N	6.4	1346.5	0.5	0.2	0.3	0.0	Artz et al. (2022)

Note. The column WTD denotes whether the additional site-specific calibration, with the water table prescribed to equal observed values, has been performed for the site (Section 2.4): Y-Yes, N-No. The mean annual air temperature (MAT) and mean annual precipitation (MAP) are calculated based on CRUJRA climate forcing data with 0.5° spatial resolution during the period from 1980 to 2020. The PFT fraction indicates the relative area fraction of peat-specific PFTs for each site. G, S, M and T represent graminoids, shrubs, mosses and lichens, and trees, respectively. Trees growing in the FI-Let site is the boreal needleleaf evergreen PFT as described in Krinner et al. (2005). More details about vegetation cover for each site can be found in Text S2 in Supporting Information S1. [a]Sedges, grasses, and herbaceous plants were grouped into graminoids in the table. [b]UK-Bal is an eroded site, but it is categorized as pristine in the analysis.

investigators or obtained from ICOS (https://www.icos-cp.eu/) or FLUXNET (https://fluxnet.org/) networks. For the data from both ICOS and FLUXNET, the mean GPP and NEE from the nighttime partition method were used, and the quality flags were used to filter data. For sites where there are gaps in climate forcing variables, 6-hourly climate forcing data from the CRU-JRA 0.5° × 0.5° global data set (Harris, 2023) were linearly interpolated and corrected to match observations and fill the gaps (Qiu et al., 2018). For precipitation, no correction was applied. At the sites SE-Hal, SE-Ham and SE-Sto, the longwave incoming radiation is unavailable from 2020 to 2022, thus the data from the nearby site SE-Deg, which is less than 3 km from each site, were used. Water table depth (WTD) was measured at 9 sites (Table 1), and gaps in WTD data were filled using two approaches. For sites where data gaps occurred due to freezing during the cold season, but observations were continuous during the growing season, and the water table was close to or above the ground surface during the shoulder season (beginning or end of the growing season), the missing WTD values were set to 0. For the FI-Sii site with small data gaps (total gap <3% of the observed period and these gaps were spread over several periods), gaps were filled by the mean values of the same period from other measurement years.

We split the observed CO_2 fluxes into two parts for model calibration (Section 2.3) and evaluation (Section 2.5), respectively (Table S1 in Supporting Information S1). For the DK-Skj (2020–2021) and UK-Bal (2018–2020) sites with very large data gaps (Figure S1 in Supporting Information S1), where both calibration and evaluation require at least one complete year, all available data were used for both calibration and evaluation. For sites with 2–3, 4 to 6, and 7–9 years of observations, the last 1, 2, and 3 years of the observation period, respectively, were used for evaluation. For the FI-Lom site with 13 years of observations, the last 4 years of observations were used. Daily-averaged observations were used for model calibration and evaluation rather than half-hourly or hourly measurements because we focused model optimization on the time scales of seasonal and interannual variability and avoided the complexity complicated treatment of the error correlations between half-hourly or hourly data (Lasslop et al., 2008). Additionally, days with less than 80% half-hourly or hourly data were excluded.

Table 2

Parameters for Model Calibration (All Corresponding Equations Are Given in Text S1 in Supporting Information S1)

Parameter	Description	PFT
Photosynthesis		
V_{cmax}	Maximum rate of carboxylation (Equations S5 and S7 in Supporting Information S1)	*G, S, M*
g_0	Stomatal conductance of mosses and lichens at no irradiance (Equation S8 in Supporting Information S1)	*M*
a_1	Empirical linear slope of the stomatal response to VPD (Equation S9 in Supporting Information S1)	*M*
b_1	Empirical intercept of the stomatal response to VPD (Equation S9 in Supporting Information S1)	*M*
LAI_{max}	Maximum leaf area index (Equation S15 in Supporting Information S1)	*G, S, M*
SLA	Specific leaf area (Equation S15 in Supporting Information S1)	*G, S, M*
Autotrophic respiration		
$C_{0,\mathrm{leaf}}$	Maintenance respiration coefficient for leaves (Equation S11 in Supporting Information S1)	*G, S, M*
GR_{frac}	Fraction of biomass allocated to growth respiration (Equation S12 in Supporting Information S1)	*G, S, M*
SOC decomposition		
τ_{peat}	Carbon decomposition rate parameter for peat vegetation (Equation S13 in Supporting Information S1)	*G, S, M*
$\mathbf{Q_{10}}$	Temperature sensitivity coefficient of the decomposition rates for all carbon pools (Equation S14 in Supporting Information S1)	-

Note. The *G*, *S*, and *M* letters in the column PFT represent graminoids, shrubs, as well as mosses and lichens, respectively. The default values and ranges for each parameter are shown in Table S2 in Supporting Information S1.

2.3. Model Calibration

We optimized 10 parameters (Table 2) controlling the fluxes of photosynthesis, autotrophic respiration and SOC decomposition at 14 European peatland sites where we collected eddy covariance observations of CO_2 and energy fluxes (Table 1 and Figure 1). While the ORCHIDEE model incorporates numerous parameters, and many of these have been optimized at site scales in recent studies (Bacour et al., 2023; Bastrikov et al., 2018; Kuppel et al., 2014; Mahmud et al., 2021; Santaren et al., 2014), we aimed to maximize model accuracy for GPP and NEE with fewer parameters that have more direct impact on key equations of photosynthesis and respiration in the model (Text S1 in Supporting Information S1). This approach reduces computational costs and improves calibration efficiency. Hence, 10 key parameters were selected, comprising nine PFT-specific parameters and one PFT-independent parameter, the $\mathbf{Q_{10}}$ temperature dependence of heterotrophic respiration. The prior values and ranges of each parameter (Table S2 in Supporting Information S1) were derived from literature data (Druel et al., 2017; Peaucelle et al., 2019; Santaren et al., 2014) and expert knowledge. It is noteworthy that out of the nine PFT-dependent parameters, three parameters (g_0, a_1 and b_1) are specific to mosses and lichens. This is because mosses and lichens have "pseudo-stomata" and it is necessary to calibrate the effect of VPD on the pseudo-stomatal conductance of mosses and lichens separately from other plant types.

The optimization of parameters to fit observed CO_2 fluxes was conducted using the ORCHIDEE data assimilation system (ORCHIDAS, Peylin et al., 2016). ORCHIDAS is specifically designed to optimize variables associated with water, energy, and carbon cycles within the ORCHIDEE LSM (Bacour et al., 2023; Kwon et al., 2022; Salmon et al., 2022). ORCHIDAS relies on the minimization of a cost function employing a Bayesian statistical formalism (Tarantola, 2005) that expresses the discrepancy between observations and simulations as well as the difference between the optimized parameter values and the prior information on them, weighted by uncertainties assigned to both observations and parameters. To minimize the cost function, a stochastic random-search method, specifically the genetic algorithm (GA), was employed. The GA, situated within the broader spectrum of

Table 3
Simulation Protocol

Simulation	S0	S1	S2	S3
PFT	Unique	Multiple	Multiple	Multiple
Calibration	–	Multi-site	Single-site	Single-site
Water table prescription	No	No	No	Yes

Note. Unique and multiple indicate that the simulations used only one C3 graminoid peat PFT and multiple peat PFTs, respectively. For the simulation S0, the parameters have been calibrated by Qiu et al. (2018). Yes or No indicates whether field observed WTD values were used to constrain peat decomposition, and this simulation was conducted only at 9 sites where field observed WTD is available (Table 1).

evolutionary algorithms and inspired by genetic and natural selection principles (Goldberg, 1989; Haupt & Haupt, 2004), facilitates the iterative refinement of the cost function. Further insights into this algorithm can be found in the study of Bastrikov et al. (2018).

In this study, the model is calibrated against daily-averaged GPP and NEE simultaneously, using equal weighting in the cost function. Observation errors were defined as the root mean square deviation (RMSD) between the observations and the prior model simulation results (Bastrikov et al., 2018; Kuppel et al., 2014). Two types of calibrations were performed over each site-specific calibration period defined in Table S1 in Supporting Information S1: (a) A single-site calibration, in which parameters were calibrated to optimize model performance at each specific location and (b) a multi-site calibration, in which a single set of parameters was optimized to optimize model performance across all locations at the same time. Both experiments were performed for 50 iterations, aiming to find the lowest cost function employing the model–data RMSD. The prior uncertainty of the parameter was set to 15% of the range of variation for each parameter following Bacour et al. (2023). Given correlation between GPP and NEE in field observations because GPP is derived from NEE after accounting for ecosystem respiration (Reichstein et al., 2005), we assessed the impact of employing all observed data versus using one daily flux data point per week in the calibration process. Results showed that using all observed data versus one flux data per week had little effect on NEE and a negligible impact on GPP calibration. For example, at the SE-Sto site (Figure S2 in Supporting Information S1), the single-site calibration employing one data per week led to a slight increase in RMSD for NEE (from 0.31 gC m^{-2} day^{-1} to 0.36 gC m^{-2} day^{-1}) and GPP (from 0.31 gC m^{-2} day^{-1} to 0.32 gC m^{-2} day^{-1}). Thus, in the model calibration, all daily data during the calibration period (Table S1 in Supporting Information S1) were used.

Water table depth (WTD) is an essential variable controlling the carbon cycle of peatlands (Chen et al., 2021; Evans et al., 2021; Zou et al., 2022). While it was only recorded at 9 sites (Table 1), we conducted an additional single-site calibration for sites where field WTD had been measured. In this extra single-site calibration, the observed WTD values were prescribed in the model, which should give more realistic hydrological conditions to constrain peat decomposition parameters (e.g., $\mathbf{Q_{10}}$).

2.4. Simulation Protocol

Four groups of simulations (S0, S1, S2, and S3) were conducted (Table 3). In S0, the previous version of the ORCHIDEE-PEAT model with only a C3 graminoid PFT to represent peat vegetation, for which parameters were previously calibrated across 30 northern peat sites (Qiu et al., 2018, 2019). S0 serves as the reference simulation (hereafter default simulation) used to evaluate modifications of the ORCHIDEE-PEAT v.3.0 model with multiple peatland PFTs (S1, S2, and S3). In S1 (multi-site calibration), parameters were simultaneously calibrated across all sites, resulting in a single set of parameters. In S2 (single-site calibration), parameters were calibrated individually for each site. In S3 (single-site calibration with prescribed WTD), the calibration was similar to S2, but the field observed water table was used to prescribe the simulated water table.

For each simulation, at each site, the model was spun up for 10,100 years, with the pre-industrial atmospheric CO_2 concentration of 285 ppm, repeated site-specific meteorological forcing, and fixed peat vegetation fractions. The spin up process comprised two steps: First, ORCHIDEE-PEAT was run for 100 years to reach the equilibrium for hydrology and soil thermal conditions, fast carbon pools, and soil carbon input from plants residue. Then a sub-model solely of soil carbon dynamics was run for 10,000 years to reach the equilibrium of soil carbon. After the soil carbon spin up, transient simulations were conducted, forced by repeated site-specific forcing and rising atmospheric CO_2 concentration from the pre-industrial level to the beginning of the respective observation period of CO_2 flux listed in Table 1. During the site-specific calibration period (Table S1 in Supporting Information S1), parameters related to GPP and NEE in S1, S2, and S3 were calibrated against observations as explained above.

2.5. Evaluation Metrics

For evaluating the model performance of each simulation (Table 3) we used the Pearson correlation coefficient (R, Equation 1), and the normalized standard deviation (nSD, Equation 2), defined as the ratio between the standard deviation of modeled values (SD_{model}, Equation 3) to that of observed values (SD_{obs}, Equation 4), and root mean square deviation (RMSD, Equation 5). Presenting all the results for all sites, Taylor diagrams (Taylor, 2001) were used to facilitate concise comparisons. These diagrams integrate standard deviation, RMSD, and R, into a single polar plot, allowing for detailed and intuitive visualization of the precision and accuracy of predictive models compared to observations. Taylor diagrams provide a clear and efficient way to compare the performance of different models (Gleckler et al., 2008).

In addition, the Akaike Information Criterion (AIC) (Akaike, 1974) was used to assess the quality of model-data fit across different simulations (S0, S1, and S2). Since the simulations involve varying numbers of optimized parameters, AIC allows for performance analysis while accounting for differences in degrees of freedom (Bazzi et al., 2024), that is the total number of optimized parameters. In this study, AIC based on weighted least squares (Equation 6) was employed (Banks & Joyner, 2017).

$$R = \frac{\sum_{i=1}^{n}(y_i - \bar{y})(\hat{y}_i - \bar{\hat{y}})}{\sqrt{\sum_{i=1}^{n}(y_i - \bar{y})^2}\sqrt{\sum_{i=1}^{n}(\hat{y}_i - \bar{\hat{y}})^2}} \tag{1}$$

$$n\mathrm{SD} = \frac{SD_{\mathrm{model}}}{SD_{\mathrm{obs}}} \tag{2}$$

$$\mathrm{SD}_{\mathrm{model}} = \sqrt{\frac{\sum_{i=1}^{n}(\hat{y}_i - \bar{\hat{y}})}{N}} \tag{3}$$

$$\mathrm{SD}_{\mathrm{obs}} = \sqrt{\frac{\sum_{i=1}^{n}(y_i - \bar{y})}{N}} \tag{4}$$

$$\mathrm{RMSD} = \sqrt{\frac{\sum_{i=1}^{n}(y_i - \hat{y}_i)^2}{N}} \tag{5}$$

$$\mathrm{AIC} = N\ln\left(\frac{\sum_{i=1}^{n} w_j^{-2}(y_i - \hat{y}_i)^2}{N}\right) + 2(p+1) \tag{6}$$

where y_i is the observed flux value, $\hat{y}_i$ is the modeled flux value, $\bar{y}$ is the mean of the observed flux values, $\bar{\hat{y}}$ is the mean of the modeled flux values. N is the total number of simulated flux values, w_j is the flux observation uncertainty, here represented by the variance, and p is the number of optimized parameters.

2.6. Assessment of the Sensitivity of Calibrated Parameters to Bioclimatic Variables

The simulations with single-site optimized parameters performed well in capturing field-observed GPP and NEE at the site scale (S1, Section 3.1). A key question is whether the optimized values of parameters at individual sites can be heuristically related to environmental conditions, allowing for the definition of new functional relationships or parameterizations that explicitly describe how parameters depend on site-specific environmental conditions. Such relationships could then be integrated into the model to represent the spatial variations of parameters and fluxes. To explore this, linear regressions were applied to evaluate the spatial gradients of the calibrated parameter values across sites in relation to bioclimatic variables, including latitude (Lati), air temperature (Tair), shortwave downward radiation (SW), and precipitation (PRE). The regressions were performed using the mean values of the bioclimatic variables computed during the simulation period (Table 1).

3. Results

3.1. Model Performance

The timeseries of observed and modeled CO_2 fluxes for four sites (CZ-Wet, DE-Zrk, FI-Sii and SE-Ham) are shown in Figure 2 as an example, and the rest can be found in Figures S3 and S4 in Supporting Information S1.

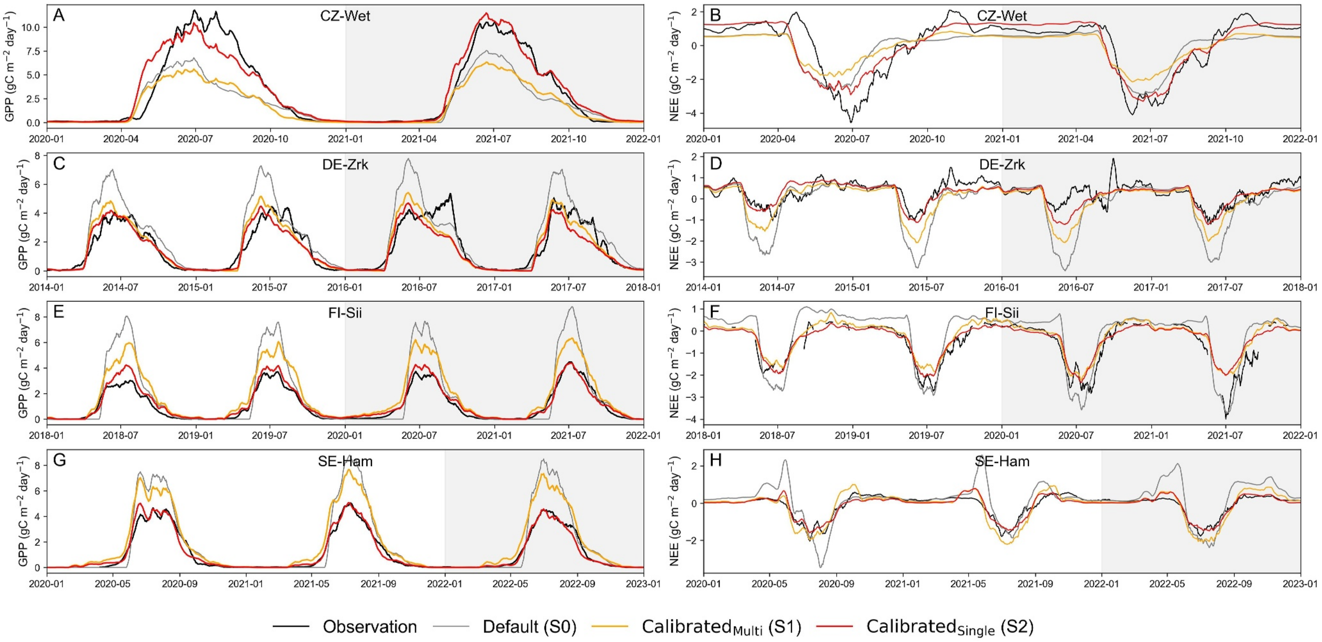

Figure 2. Timeseries of gross primary production and NEE for (a–b) CZ-Wet (c–d) DE-Zrk, (e–f) FI-Sii and (g–h) SE-Ham. The plots have been smoothed by a running mean with a window equal to 15 days. The gray shading in each plot indicates the period used to calculate evaluation metrics (Table S1 in Supporting Information S1).

The single-site calibrated simulations (S2, red lines) demonstrate substantially improved model performance in capturing field observations for both GPP and NEE compared to the default simulations (S0, gray lines). As expected, the multi-site calibrated simulations (S1, orange curves) display an intermediate performance. This improvement is particularly visible in the simulated magnitude of GPP. Default simulation significantly underestimates GPP at the CZ-Wet site, whereas it is overestimated at the other three sites, especially during the growing season. The multi-site calibration reduces this discrepancy slightly, but single-site calibration closely fits all field observations, particularly at the FI-Sii and SE-Ham sites (Figures 2e and 2g). In addition, the improved vegetation composition leads to better model performance in capturing seasonal variations in GPP and NEE. For instance, at the SE-Ham site (Figures 2g and 2h), during the shoulder seasons (the beginning and the end of the growing season), modeled GPP and NEE from the new model version with multiple PFTs (S1 and S2) accurately reflect field observations compared to the model version with only one C3 graminoid PFT (S0).

Taylor diagrams are shown in Figure 3, and statistics are calculated using daily data from the evaluation period for each site in Table S1 in Supporting Information S1. In the default simulations using only one graminoid PFT (S0), the correlation coefficient (R, Equation 1) between simulated and observed daily GPP ranges from 0.67 to 0.97 (Figure 3), with a mean value of 0.91 ± 0.08 (±σ, standard deviation across 14 sites). This mean R-value is smaller than that of the simulations using multi-site optimized parameters (S1) ranging from 0.60 to 0.99 (mean $R = 0.92 \pm 0.10$) and using single-site optimized parameters (S2) ranging from 0.71 to 0.99 (mean $R = 0.94 \pm 0.07$). A similar pattern is observed in NEE simulations, with mean R-values of 0.84 ± 0.08 (range: 0.68 to 0.93), 0.88 ± 0.09 (range: 0.68 to 0.98) and 0.88 ± 0.08 (range: 0.70 to 0.97) for the default simulations, simulations using multi-site optimized parameters and simulations using single-site optimized parameters, respectively (Table S3 in Supporting Information S1).

The normalized standard deviation (nSD, Equation 2) in Figure 3, calculated as the ratio between the standard deviation of the modeled values (SD_{model}, Equation 3) and that of the observed values (SD_{obs}, Equation 4), serves as a metric for evaluating the model's ability to capture observed variability. A value of nSD greater than 1 indicates that the variability in the simulation exceeds that of the observation (nSD>1), and vice versa. Results show that, in default simulations, the ranges and mean values of nSD are 0.50–2.35 and 1.32 ± 0.58 for GPP, and 0.43 to 2.49 and 1.35 ± 0.65 for NEE, indicating that the modeled variability of both GPP and NEE are significantly overestimated in these simulations. This overestimation, as quantified by nSD, is significantly reduced in the multi-site calibrated simulations, with ranges and mean values of nSD are 0.59–1.78, 1.05 ± 0.38 and 0.50 to 1.57,

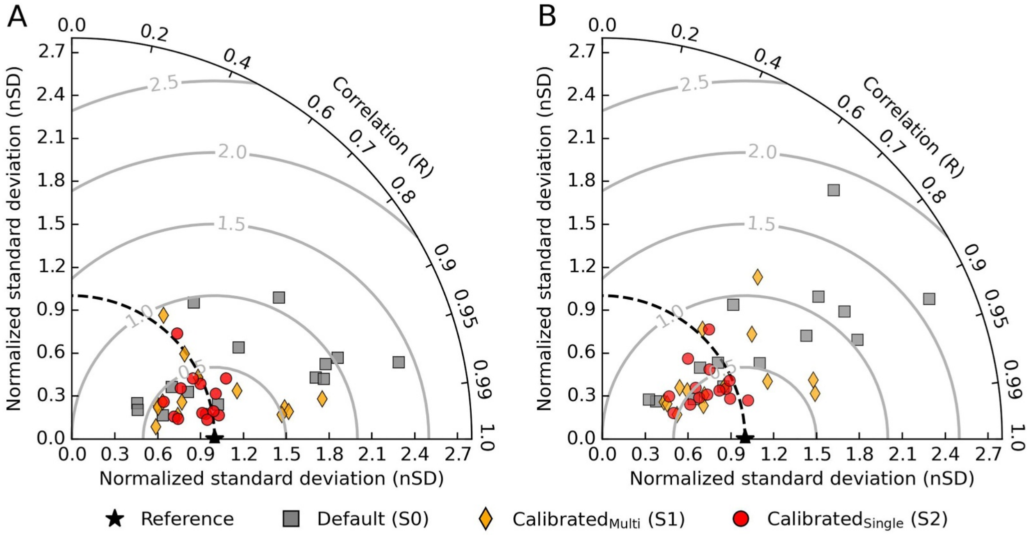

Figure 3. Taylor diagram of (a) gross primary production (GPP) (gC m^{-2} day^{-1}) and (b) NEE (gC m^{-2} day^{-1}) for default (S0, gray square), multi-site calibrated (S1, orange diamond) and single-site calibrated (S2, red circle) simulations. Statistics were calculated using daily data of the evaluation period for each site (Table S1 in Supporting Information S1). All points were normalized by dividing the standard deviation of model results by the standard deviation of the corresponding measurements (nSD, unitless); thus, the reference point is 1.0. Timeseries plots of both GPP and NEE for each site are shown in Figures S3 and S4 in Supporting Information S1, respectively.

0.97 ± 0.38 for GPP and NEE respectively (Table S3 in Supporting Information S1). In contrast, the single-site calibrated simulations exhibit a slight underestimation of the observed variability for both GPP (nSD ranging from 0.69 to 1.16, mean nSD = 0.94 ± 0.13) and NEE (nSD ranging from 0.53 to 1.07, mean nSD = 0.83 ± 0.16) (Table S3 in Supporting Information S1).

The RMSD (Equation 5) between modeled and observed GPP reduces by approximately 22% and 53% from the default simulations of 1.67 ± 0.69 gC m^{-2} day^{-1} to 1.30 ± 0.67 gC m^{-2} day^{-1} in multi-site calibrated simulations, and further to 0.78 ± 0.50 gC m^{-2} day^{-1} in single-site calibrated simulations, respectively. For NEE, the RMSD values decrease by about 23% and 40%, from 0.84 ± 0.29 gC m^{-2} day^{-1} for the default simulations to 0.65 ± 0.34 gC m^{-2} day^{-1} and 0.50 ± 0.28 gC m^{-2} day^{-1} for the multi-site calibrated and the single-site calibrated simulations, respectively (Table S3 in Supporting Information S1).

We further analyzed the model performance at a yearly timescale, using data from all observed periods. For the sites with gaps in field observations, we identified a valid year as containing data over at least 339 days in a 365-day period. We then aggregated daily fluxes into an annual scale for both modeled and observed data during each valid year (Table S4 in Supporting Information S1). Finally, we calculated the mean annual fluxes over multiple years (Figure 4). There was only one valid year was identified for the DK-Skj and UK-Bal sites. The GL-NuF site was excluded from this analysis due to its field observations being limited to the growing season and having gaps exceeding 50% each year (Figures S3 and S4 in Supporting Information S1). The single-site calibrated simulations of annual GPP (mean value = 734.1 ± 407.7 gC m^{-2} year^{-1}) show a better match with observations (mean value = 711.2 ± 392.9 gC m^{-2} year^{-1}), than the multi-site calibrated simulations (mean value = 678.8 ± 204.8 gC m^{-2} year^{-1}). In contrast, default simulations significantly underestimated annual GPP at 4 sites (CZ-Wet, DE-Akm, DK-Skj and FI-Let) and overestimated GPP at 6 sites (DE-Zrk, FI-Sii and the four SE-sites). For annual NEE, model performance has the most significant improvement at the DE-Zrk, FR-LGt and UK-Bal sites using single-site calibrated parameters. At these three sites, simulations using single-site optimized parameters match with observations, indicating that they act as carbon sources (positive values), whereas default and multi-site calibrated simulations suggested they are all carbon sinks (negative values). In addition, the multi-site calibrated simulations have better performance at DE-Akm, FI-Lom, SE-Deg, SE-Hal, and SE-Sto sites than the default simulations.

The impact of the water table on the carbon cycle of peatlands has been well-documented (Chen et al., 2021; Evans et al., 2021; Zou et al., 2022). In this study, we conducted an additional single-site optimization experiment

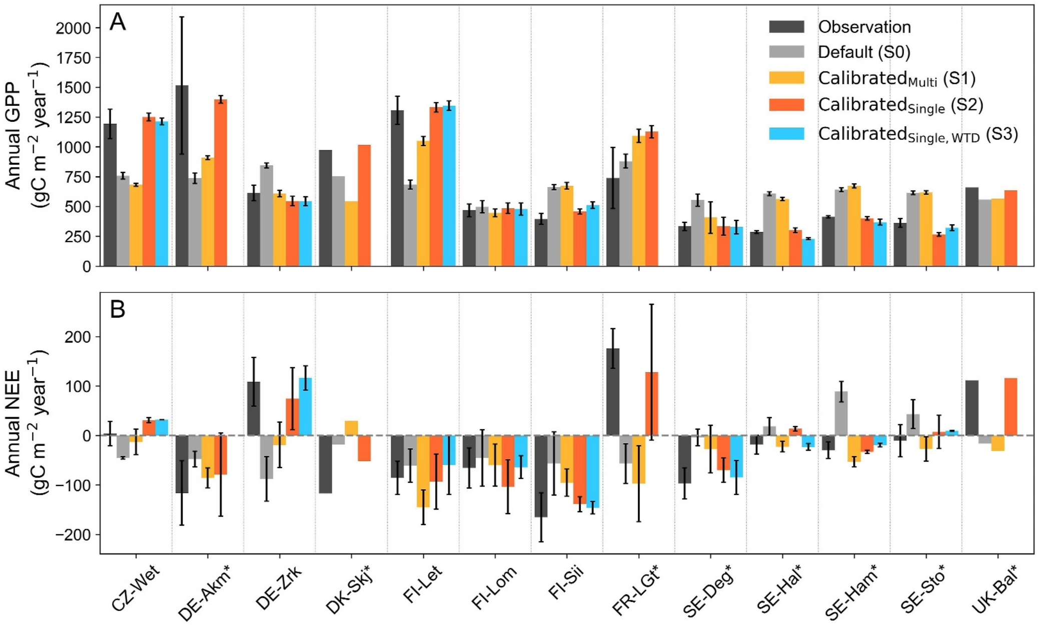

Figure 4. Comparison of observed and modeled fluxes at the annual scale. (a) gross primary production, (b) NEE. The error bars represent the SD.* indicates the site where field observation has data gaps, and annual fluxes were calculated from the periods with 365 continuous days (e.g., 20 December 2020 to 19 December 2021 for DK-Skj site). Periods and total years used to calculate the mean annual values for sites with gaps are shown in Table S4 in Supporting Information S1. The light blue bars represent the results from single-site calibration with prescribed Water table depth (WTD) for 9 sites where field observed WTD is available (Table 1).

at 9 sites where the observed WTD data was available and used directly to force the model (Table 1). When prescribing the observed WTD, the performance of simulated GPP weakened slightly compared to the standard single-site calibration simulations (S2), where WTD is internally simulated by the model. Specifically, the nSD decreased from 0.96 ± 0.11 (median ± σ) to 0.86 ± 0.11 and the RMSD value increased from 0.41 ± 0.27 to 0.44 ± 0.24 (Figure 5 and Table S3 in Supporting Information S1). Conversely, the model performance for NEE improved slightly with prescribed WTD. The nSD increased from 0.89 ± 0.17 to 0.92 ± 0.18, and the RMSD value decreased from 0.42 ± 0.14 gC m^{-2} day^{-1} to 0.39 ± 0.16 gC m^{-2} day^{-1}. At the annual scale, the improvement of model performance for NEE with prescribed WTD is more evident at 5 out of the 9 sites (DE-Zrk, FI-Lom, FI-Sii, SE-Deg and SE-Hal, Figure 4b). This improvement can be attributed to two factors: first, the soil moisture profile controlling peat carbon decomposition in the model (Equation S13 in Supporting Information S1) (Ise et al., 2008; Ise & Moorcroft, 2006), and second, the organic matter content and associated hydro-physical properties of the soil are directly influenced by the WTD (Ahmad et al., 2020; Górecki et al., 2021). Prescribing

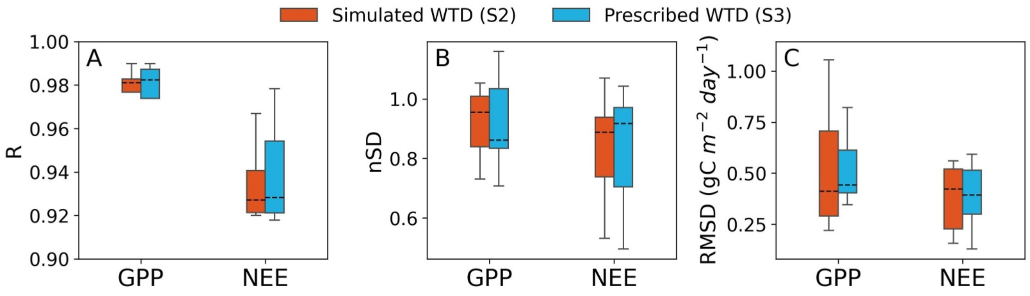

Figure 5. Comparison of modeled gross primary production and NEE between the standard single-site calibration (S2, red boxes) and the single-site calibration with prescribed Water table depth (S3, blue boxes). (a) Pearson correlation coefficient (*R*), (b) normalized standard deviation and (c) root mean square deviation. The dark dashed lines in the boxes represent the median value. Statistics were calculated using daily data of the evaluation period for each site (Table S1 in Supporting Information S1).

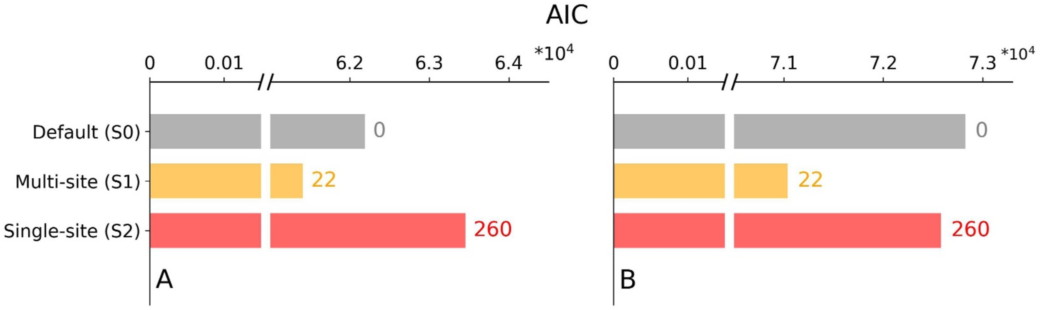

Figure 6. Akaike Information Criterion for the default simulations (S0, gray), multi-site calibrated simulations (S1, orange) and single-site calibrated simulations (S2, red) calculated using daily data for (a) gross primary production and (b) NEE. The numbers beside each bar correspond to the number of parameters optimized for each experiment. Statistics were calculated using daily data of the evaluation period for each site (Table S1 in Supporting Information S1).

WTD therefore introduces more realistic variations in soil moisture and water table levels, resulting in a more accurate simulation of SOC decomposition and accumulation processes.

Compared with the single-site calibration (S2), which involved optimizing a total of 260 parameter values for the 14 sites, the multi-site calibration (S1), with only 22 parameters optimized, has a worse performance in simulating CO_2 fluxes. To better evaluate the performance of the model between the default simulation (S0), the multi-site calibrated simulation (S1) and the single-site calibrated simulation (S2), the AIC of weighted least squares (AIC, Equation 6) shown in Figure 6 illustrates that the single-site calibration (S2) has higher AIC scores for GPP and slightly lower scores for NEE compared to the default simulation. This indicates that despite the significantly increased degree of freedom, results from the single-site calibration remain robust for NEE, without suffering from overfitting, but GPP parameters may be over-fitted. While the single-site calibration (S2) promotes more significant performance improvement of the model at each location (Figure 3, Table S3 in Supporting Information S1), in regional- or large-scale simulation, a single set of parameters must be used across all locations. The multi-site calibration (S1) exhibits the lowest AIC value for both GPP and NEE compared to the other experiments. This indicates that at the scale encompassing all 14 sites, multi-site calibrated simulation outperforms both default and single-site calibrated simulation.

3.2. Spatial Gradients in Optimization Parameters Across Sites

The correlation coefficients (R) of the linear regression between each optimized parameter, obtained from single-site calibration, and bioclimatic variables, including latitude (Lati), air temperature (Tair), short wave incoming

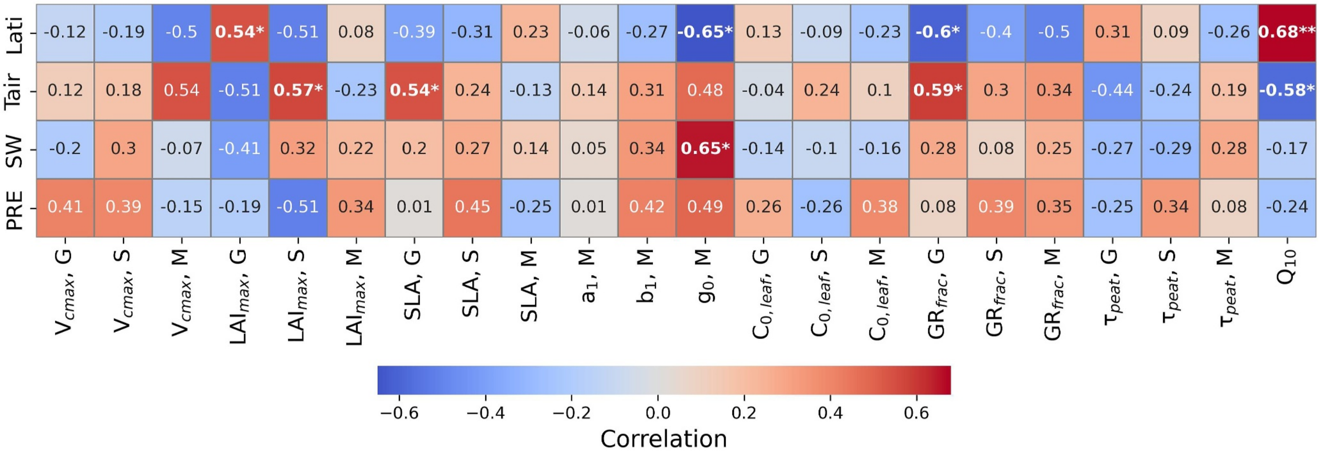

	V_{cmax}, G	V_{cmax}, S	V_{cmax}, M	LAI_{max}, G	LAI_{max}, S	LAI_{max}, M	SLA, G	SLA, S	SLA, M	a_1, M	b_1, M	g_0, M	$C_{0,leaf}$, G	$C_{0,leaf}$, S	$C_{0,leaf}$, M	GR_{frac}, G	GR_{frac}, S	GR_{frac}, M	τ_{peat}, G	τ_{peat}, S	τ_{peat}, M	Q_{10}
Lati	-0.12	-0.19	-0.5	**0.54***	-0.51	0.08	-0.39	-0.31	0.23	-0.06	-0.27	**-0.65***	0.13	-0.09	-0.23	**-0.6***	-0.4	-0.5	0.31	0.09	-0.26	**0.68****
Tair	0.12	0.18	0.54	-0.51	**0.57***	-0.23	**0.54***	0.24	-0.13	0.14	0.31	0.48	-0.04	0.24	0.1	**0.59***	0.3	0.34	-0.44	-0.24	0.19	**-0.58***
SW	-0.2	0.3	-0.07	-0.41	0.32	0.22	0.2	0.27	0.14	0.05	0.34	**0.65***	-0.14	-0.1	-0.16	0.28	0.08	0.25	-0.27	-0.29	0.28	-0.17
PRE	0.41	0.39	-0.15	-0.19	-0.51	0.34	0.01	0.45	-0.25	0.01	0.42	0.49	0.26	-0.26	0.38	0.08	0.39	0.35	-0.25	0.34	0.08	-0.24

Figure 7. Correlation between calibrated parameters from single-site calibration and latitude of the site location (Lati), air temperature (Tair), shortwave downward radiation (SW), as well as precipitation (PRE). The corresponding scatter plots are shown in Figures S5 to S8 in Supporting Information S1. * and ** indicate the $P \leq 0.05$ and $P \leq 0.01$, respectively. The *G*, *S*, and *M* represent graminoids, shrubs, and mosses and lichens, respectively.

radiation (SW), and precipitation (PRE), are shown in Figure 7, and corresponding plots are shown in Figures S5 to S8 in Supporting Information S1. Although most of the regressions revealed non-significant correlations ($P > 0.05$), the regressions provide a basis for analyzing gradient variations among different parameters for each PFT. Furthermore, it is worth noticing that the gradient patterns involved by both Tair (Figure S6 in Supporting Information S1) and SW (Figure S7 in Supporting Information S1) could also be attributed to differences in latitudinal positions, as both SW ($R = -0.93$, $P < 0.01$) and Tair ($R = -0.67$, $P < 0.01$) exhibits a linear decrease with increasing latitude (Figure S9 in Supporting Information S1).

We found that climatic conditions are influencing parameters related to photosynthesis. The leaf maximum photosynthesis rate ($\boldsymbol{V}_{\mathbf{cmax}}$) for three PFTs has a positive correlation with air temperature (Tair) and a negative correlation with latitudinal position This implies that peatland vegetation trends to have higher $\boldsymbol{V}_{\mathbf{cmax}}$ where there is higher temperature in lower latitudes, particularly for mosses and lichens which exhibit a stronger positive relationship between $\boldsymbol{V}_{\mathbf{cmax}}$ and air temperature (Tair) ($R = 0.54$, $P = 0.11$) than graminoids ($R = 0.12$, $P = 0.67$) and shrubs ($R = 0.18$, $P = 0.59$). While $\boldsymbol{V}_{\mathbf{cmax}}$ has a stronger positive correlation with precipitation (PRE) for both graminoids ($R = 0.41$, $P = 0.15$) and shrubs ($R = 0.39$, $P = 0.21$), suggesting that higher precipitation amount enhances the maximum rate of carboxylation for graminoids and shrubs in peatlands. The parameter of maximum leaf area index ($\boldsymbol{LAI}_{\mathbf{max}}$) for graminoids exhibits a negative correlation with both Tair ($R = -0.51$, $P = 0.06$) and SW ($R = -0.41$, $P = 0.15$), and a positive correlation with latitude ($R = 0.54$, $P \leq 0.05$). These correlations suggest that higher temperatures or light levels decrease the $\boldsymbol{LAI}_{\mathbf{max}}$ of graminoids. In contrast, it has the opposite behavior for shrubs where $\boldsymbol{LAI}_{\mathbf{max}}$ shows a positive correlation with both Tair ($R = 0.57$, $P \leq 0.05$) and SW ($R = 0.32$, $P = 0.31$), and a negative correlation with latitude ($R = -0.51$, $P = 0.09$). In addition, it shows a negative correlation with PRE ($R = -0.51$, $P = 0.09$), implying that excess precipitation may constrain the $\boldsymbol{LAI}_{\mathbf{max}}$ of shrubs. Specific leaf area of graminoids and shrubs, which is a parameter influencing the LAI (Equation S15 in Supporting Information S1), demonstrates stronger correlations with Tair and PRE than for mosses and lichens. In particular, the ***Specific leaf area*** of graminoids and shrubs show a positive correlation with Tair ($R = 0.54$, $P \leq 0.05$) and PRE ($R = 0.45$, $P = 0.14$), respectively. For the three parameters ($\boldsymbol{a_1}$, $\boldsymbol{b_1}$ and $\boldsymbol{g_0}$) associated with the stomatal conductance ($\boldsymbol{g_s}$) of mosses and lichens (Equation S9 in Supporting Information S1). Both $\boldsymbol{g_0}$ and $\boldsymbol{b_1}$ have stronger correlations with bioclimate variables than that of $\boldsymbol{a_1}$. Specifically, the parameter $\boldsymbol{g_0}$, which defines the baseline stomatal conductance at zero light, shows a positive correlation with SW ($R = 0.65$, $P \leq 0.05$) and PRE ($R = 0.49$, $P = 0.15$), while the parameter $\boldsymbol{b_1}$, which hinders stomatal conductance, also demonstrates a positive sensitivity to SW ($R = 0.34$, $P = 0.34$) and PRE ($R = 0.42$, $P = 0.22$). These findings suggest that the stomatal conductance of mosses and lichens is sensitive to increased light and precipitation intensity while it may have a complex mechanism in response to climate.

For two parameters ($\mathbf{GR}_{\mathbf{frac}}$ and $\boldsymbol{C}_{\boldsymbol{0},\mathbf{leaf}}$) related to autotrophic respiration. The analysis from $\boldsymbol{GR}_{\mathbf{frac}}$, the parameter defining the proportion of biomass consumed by growth respiration (Equation S12 in Supporting Information S1), shows that it has a positive correlation with air temperature (Tair) across all three PFTs. This correlation is particularly strong for graminoids, with a significant positive correlation ($R = 0.59$, $P \leq 0.05$), suggesting that higher temperatures lead to increased biomass consumption through growth respiration. Conversely, $\boldsymbol{C}_{\boldsymbol{0},\mathbf{leaf}}$, the parameter representing the maintenance respiration coefficient for leaves (Equation S11 in Supporting Information S1), exhibits less sensitivity to bioclimate variables compared to $\mathbf{GR}_{\mathbf{frac}}$. However, for mosses and lichens, both $\boldsymbol{GR}_{\mathbf{frac}}$ and $\boldsymbol{C}_{\boldsymbol{0},\mathbf{leaf}}$ are positively correlated with PRE ($R = 0.38$ for $\boldsymbol{C}_{\boldsymbol{0},\mathbf{leaf}}$ and $R = 0.35$ $\boldsymbol{GR}_{\mathbf{frac}}$, $P \geq 0.05$ for both), suggesting higher precipitation level may enhance autotrophic respiration under warm condition.

Regarding the parameters controlling SOC decomposition. The parameter $\boldsymbol{\tau}_{\mathbf{peat}}$, representing the carbon decomposition rate for peatland vegetation (Equation S13 in Supporting Information S1), has negative correlation with Tair and SW for graminoids (R are -0.44 and -0.27, $P > 0.05$ for both) and shrubs (R are -0.24 and -0.29, $P > 0.05$ for both), indicating that carbon decomposition is faster with increased temperature or light intensity. The parameter $\mathbf{Q}_{\mathbf{10}}$, by which respiration rates increase for a 10°C increase in temperature, is robustly correlated to both latitudinal position ($R = 0.68$, $P \leq 0.01$) and Tair ($R = -0.58$, $P \leq 0.05$). Both $\boldsymbol{\tau}_{\mathbf{peat}}$ and $\mathbf{Q}_{\mathbf{10}}$ demonstrate a strong sensitivity of soil carbon decomposition to temperature across the latitudinal gradient of sites. We remind that the spatial variations of soil carbon decomposition parameters will imply a different response to future warming. For example, there may be more CO_2 emissions for a unit warming at high latitudes compared to low latitudes for the same WTD.

4. Discussion

4.1. Biochemical Mechanisms Reflected From Optimized Parameters

From the single-site calibration, we observed that, for all PFTs, optimized $\boldsymbol{V_{\mathbf{cmax}}}$ has a positive linear correlation with air temperature and a negative linear correlation with latitude (Figure 7, Figures S5 and S6 in Supporting Information S1). This result aligns with findings from Walker et al. (2017), who noted a decrease in $\boldsymbol{V_{\mathbf{cmax}}}$ with increasing latitude in the Northern Hemisphere, attributing it to nitrogen (N) uptake constraints, which are influenced by soil carbon and nitrogen recycling, and mean annual temperature. The relationship between $\boldsymbol{V_{\mathbf{cmax}}}$ and latitude (temperature) identified in our study likely stems from two key factors. First, sites at lower latitudes have longer growing seasons and higher temperatures, which enhances vegetation productivity (Fang et al., 2003; Nemani et al., 2003; Piao et al., 2007). Second, higher temperatures increase nutrient availability by promoting plant litter decomposition and nitrogen release, although litter decomposition is also influenced by soil moisture, vegetation type, litter quality, and its interactions with temperature (Aerts, 2006; Cornelissen et al., 2007; Gogo et al., 2016). Since nitrogen is essential for proteins involved in photosynthesis, the photosynthetic capacity is highly correlated with N availability (Evans, 1989; Takashima et al., 2004; Walker et al., 2014). Although the nitrogen cycle is not explicitly modeled in ORCHIDEE-PEAT, the relationship between $\boldsymbol{V_{\mathbf{cmax}}}$ and latitude (temperature) may indirectly reflect the influence of nitrogen on photosynthesis rates.

Previous studies suggested that autotrophic respiration, comprising both growth and maintenance respirations, is highly sensitive to temperature variations (Juszczak et al., 2013; Lafleur et al., 2005). This sensitivity is particularly notable in peatlands with vascular plants which can access deeper water through root systems (Murphy & Moore, 2010). In contrast, non-vascular species such as mosses, which lack root systems accessing deeper water (Nijp et al., 2014), are more responsive to precipitation levels (Porada et al., 2018; Robroek et al., 2009). Consistent with these observations, our findings show that graminoids exhibit increased biomass consumption through growth respiration in response to rising temperatures, as evidenced by the positive significant correlation between $\mathbf{GR_{frac}}$ and Tair ($R = 0.59$, $P < 0.05$) (Figure 7 and Figure S6 in Supporting Information S1). In contrast, growth ($\boldsymbol{C_{0,\mathbf{leaf}}}$) and maintenance ($\mathbf{GR_{frac}}$) respiration parameters in mosses and lichens show greater sensitivity to precipitation ($R = 0.38$ for $\boldsymbol{C_{0,\mathbf{leaf}}}$ and $R = 0.35$ for $\mathbf{GR_{frac}}$, $P > 0.05$ for both) than to temperature ($R = 0.1$ for $\boldsymbol{C_{0,\mathbf{leaf}}}$ and $R = 0.34$ for $\mathbf{GR_{frac}}$, $P > 0.05$ for both) (Figure 7, Figures S6 and S8 in Supporting Information S1). These results align with the studies cited above, suggesting that autotrophic respiratory responses to environmental factors vary among different functional types of plants.

The constant $\mathbf{Q_{10}}$ values are used in most land surface and dynamic vegetation models, but recent findings suggest that the $\mathbf{Q_{10}}$ may be higher in cold climate regions (Byun et al., 2021; Koven et al., 2017; Peng et al., 2009). In this study, we found robust negative linear correlation between optimized $\mathbf{Q_{10}}$ and temperature ($R = -0.58$, $P < 0.05$) (Figure 7 and Figure S6 in Supporting Information S1), which is consistent with previous work that reports lower temperature sensitivities of the decomposition of soil organic matter under warmer climate conditions (Fang et al., 2005; Hilasvuori et al., 2013; Koven et al., 2017; Li, Nie, et al., 2020, Li, Pei, et al., 2020). Several mechanisms have been identified to explain why $\mathbf{Q_{10}}$ values are lower at higher temperatures, related to ecosystem thermal acclimation and the lower quality of organic matter. These include biochemical adjustments, such as the decreasing capacity of microbes to surmount enzyme activation energies with rising temperatures (Ma et al., 2023; Smith & Dukes, 2013), and structural changes like alterations in community composition or reductions in microbial biomass (Atkin & Tjoelker, 2003; Bradford et al., 2008; Niu et al., 2012). Furthermore, other studies highlight increasing constraints on substrate availability for decomposers as a significant limiting factor at warmer sites (Hartley et al., 2009; Ågren & Wetterstedt, 2007). These studies indicate that multiple mechanisms, each contributing at varying degrees, influence the $\mathbf{Q_{10}}$ dependence on temperature in different environmental contexts (Davidson & Janssens, 2006; Niu et al., 2021).

4.2. Impact of Incorporating Calibration Derived Trait–Climate Relationships Into the Model

In most LSMs, constant parameter values are used to prescribe trait-related or process-related parameters of a given PFT, derived from discrete observations (Kattge et al., 2009; Reich et al., 2007). This rigid parameter values overlooks the fact that climate can modulate plant traits in the real world (Maire et al., 2015; Ordoñez et al., 2009; van Ommen Kloeke et al., 2012; Wright et al., 2005). Consequently, this limitation hinders the improvement of model performance through generic optimization in large-scale simulations. This is evident in our results, where the model did not show significant performance improvement in simulating CO_2 fluxes in the multi-site

Table 4
Statistics of Root Mean Square Deviation (Median ± σ, Unit: gC m^{-2} Day^{-1}) Between Field Observations and Simulations for Gross Primary Production (GPP) and NEE Across 10 Sites, Where There is Mosses or Lichens Growth (Table 1)

	RMSD	
Variable	Multi-site	Multi-site-new
GPP	1.08 ± 0.36	0.85 ± 0.42
NEE	0.52 ± 0.22	0.44 ± 0.27

Note. Statistics were calculated using daily data of the evaluation period for each site (Table S1 in Supporting Information S1). Multi-site represents the simulations using multi-site optimized parameters (S1). Multi-site-new represents simulation using multi-site optimized parameters and the developed model which incorporates correlations between $\mathbf{Q_{10}}$, mosses' $\boldsymbol{V_{cmax}}$ and Tair.

calibration (Figures 2 and 3, Table S3 in Supporting Information S1). To address this, we use the $\mathbf{Q_{10}}$ and $\boldsymbol{V_{cmax}}$ parameters as examples to demonstrate that model accuracy at the regional scale can be enhanced by incorporating trait-climate relationships diagnosed from single site optimizations. Specifically, the negative linear relationship between $\mathbf{Q_{10}}$ and mean air temperature (Tair) (Figure S6J in Supporting Information S1, $R = -0.58$, $P \leq 0.05$), and the positive linear relationship between $\boldsymbol{V_{cmax}}$ and Tair for mosses and lichens (Figure S6C in Supporting Information S1, $R = 0.54$, $P = 0.11$) derived from the single site calibration simulations were incorporated into ORCHIDEE-PEAT v.3.0, and an additional set of simulations across 10 sites, where there is mosses or lichens growth (Table 1), have been conducted, in which the multi-year mean air temperature from the observation period for each site was used to define the relationships (Table 1).

The results show that for those 10 sites, the performance of the model is improved when the two trait-climate relationships are incorporated. Specifically, the RMSD of GPP and NEE are decreased from 1.08 ± 0.36 gC m^{-2} day^{-1} (median ± σ) to 0.85 ± 0.42 gC m^{-2} day^{-1} and from 0.52 ± 0.22 gC m^{-2} day^{-1} to 0.44 ± 0.27 gC m^{-2} day^{-1}, respectively (Table 4). In addition, regarding annual GPP and NEE (Figure S10 in Supporting Information S1), with data from 9 available sites (Table S4 in Supporting Information S1), the results show improved performance for annual GPP at 7 of the 9 sites (Figure S10A in Supporting Information S1). This improvement is less pronounced for annual NEE, with only 7 out of 9 sites having the right sign of simulated annual NEE after optimization (Figure S10B in Supporting Information S1). At two sites (FR-LGt and UK-Bal), the inclusion of trait-climate relationships in the model optimization led to NEE being annual carbon sinks (negative values, Figure S10B in Supporting Information S1), whereas single-site calibrated simulations (S2) and observations indicated carbon sources as observed (positive values, Figure 4b). This bias arises because NEE is calculated by subtracting autotrophic and heterotrophic respirations from GPP. While incorporating trait-climate correlations improved processes GPP, additional trait-climate relationships controlling autotrophic and heterotrophic respirations were not included in this experiment, contributing to observed discrepancies for mean annual NEE. Furthermore, the optimization focused on fitting daily flux variability, and despite improvements, residual errors in daily values were significant enough to cause deviations in mean annual NEE from observed data. We outline here that we do not aim to force the model to simulate annual NEE but to fit daily value.

In summary, these results underline the feasibility and importance of including trait dependencies on climate into LSMs. Such integration is essential for accurately modeling ecosystem dynamics across temporal and spatial scales, as well as their response to global drivers such as climate, elevated CO_2 and nutrient fertilization (Atkin et al., 2015; Hartig et al., 2012; Kroner & Way, 2016; Reich et al., 2016).

4.3. Impact of WTD on SOC Decomposition Parameter

Soil moisture, which is correlated to WTD, is a crucial factor indirectly affecting the optimization of the temperature sensitivity of SOC decomposition ($\mathbf{Q_{10}}$ in the model) in peatlands (Byun et al., 2021; Davidson & Janssens, 2006; Fairbairn et al., 2023; Wang et al., 2006). Across 9 sites where field observed WTD data are available, the observed multi-year median WTD ranges from −39.8 to 47.4 cm (negative value indicates water table is below the soil surface), while modeled WTD ranges from −24.5 to −1.9 cm. The modeled WTD (mean value = −7.8 ± 7.6 cm) is generally lower than that of field observation (mean value = −0.9 ± 20.8) for the 9 sites (Table S7 in Supporting Information S1). Results from our single-site calibration show that, after prescribing WTD with field observations, the value of optimized $\mathbf{Q_{10}}$ ($\mathbf{Q_{10,prescribe}}$, mean value = 1.76 ± 0.53) is generally smaller than that from the standard single-site calibration ($\mathbf{Q_{10,model}}$, mean value = 3.82 ± 1.92), in which internally simulated WTD is used (Table S7 in Supporting Information S1). This finding aligns with previous studies which showed that lower soil moisture or lower WTD tends to increase the $\mathbf{Q_{10}}$ of peat decomposition (Hardie et al., 2011; Szafranek-Nakonieczna & Stêpniewska, 2014), especially at the SE-Deg and SE-Ham sites, where modeled WTDs were significantly lower than field observations, $\mathbf{Q_{10,model}}$ are more than two times larger than $\mathbf{Q_{10,obs}}$ (Table S7 in Supporting Information S1). Moreover, at the individual site scale, especially for the 7 pristine sites, the optimized $\mathbf{Q_{10}}$ increases as the corresponding WTD decreases (Figure 8), consistent with findings that drier conditions (i.e., lower WTD) enhance the temperature sensitivity of SOC decomposition (Chen

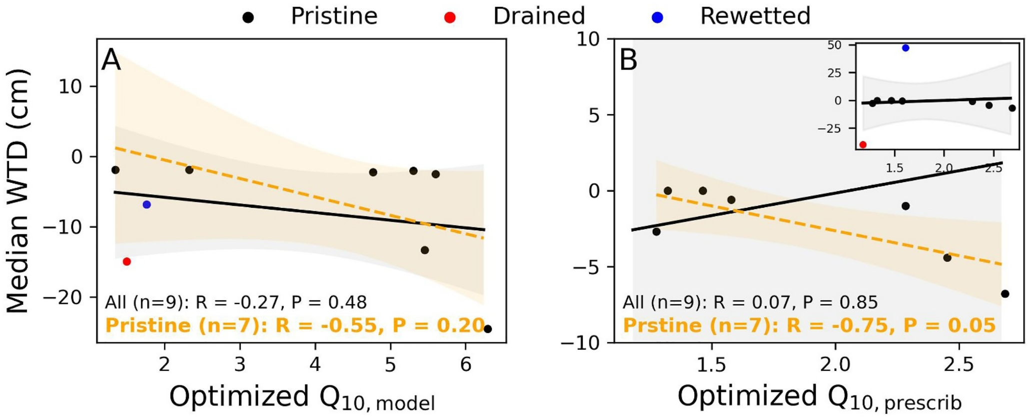

Figure 8. Correlation between optimized $\mathbf{Q_{10}}$ from single-site calibration and corresponding Water table depth (WTD). (a) Optimized $\mathbf{Q_{10}}$ ($\mathbf{Q_{10,model}}$) with model internal simulation WTD (b) optimized $\mathbf{Q_{10}}$ ($\mathbf{Q_{10,prescrib}}$) with field observed WTD. Median WTD is the multi-year mean water table for each site and the negative value represents the water table below the ground surface. Solid dark and dashed orange lines represent the linear regression for the 9 data points and 7 data points that excluded FI-Let (drained site, modeled and observed multi-year median WTD are −14.9 and −39.8 cm, respectively) and DE-Zrk (rewetted site, modeled and observed multi-year median WTD are −6.8 and 47.4 cm, respectively), respectively. The regular and bold text are correlation coefficients and corresponding p-values for linear regressions for all data points and 7 data points, respectively. The colored shadings represent the 95% confidence interval. The values of each data point are shown in the Table S7 in Supporting Information S1.

et al., 2018; Liu et al., 2024). It suggests that under the trend of peatlands drying from natural climate change in some areas (Swindles et al., 2019; Xi et al., 2021) and global warming (Cook et al., 2014), CO_2 emissions and evapotranspiration (ET) from peatlands are likely to increase (Grosse et al., 2011; Helbig et al., 2020). Peatland rewetting, achieved by raising the water table close to the surface, is advocated as a viable strategy for curbing CO_2 emissions from peatlands when the water table is no more than 20 cm from the ground surface (Evans et al., 2021). The correlation between WTD and the optimized $\mathbf{Q_{10}}$ (Figure 8, Table S7 in Supporting Information S1) suggests that peatland rewetting could additionally mitigate climate change by lowering $\mathbf{Q_{10}}$ values under wet conditions.

4.4. Uncertainties and Outlook

Degradation (e.g., drainage) and restoration (e.g., rewetting) will lead to changes in hydro-physical properties of peatland (Liu et al., 2020; Menberu et al., 2016; Morris et al., 2011; Wang et al., 2021), results in different GHG exchange than pristine peatlands (Laine et al., 2019; Renou-Wilson et al., 2019; Zou et al., 2022). In this study, 2 rewetted (DK-Skj, DE-Zrk) and 2 drained (FI-Let, FR-LGt) sites were included in the calibration, together with 10 pristine sites, which brings uncertainties on the multi-site calibration results (S1). To address this bias, additional multi-site calibration was conducted, in which only the 10 pristine sites were used. The results show that there was no significant difference between the multi-site calibration using all sites (S1) and the one using the 10 pristine sites only (Table S8 in Supporting Information S1). For GPP (and NEE), the average *R*, nSD and RMSD are 0.92 ± 0.12 (0.89 ± 0.09), 1.16 ± 0.39 (0.98 ± 0.38), and 1.26 ± 0.71 (0.61 ± 0.39) gC m^{-2} day^{-1} respectively for multi-site calibration using all sites, and 0.93 ± 0.12 (0.90 ± 0.08), 1.20 ± 0.37 (0.99 ± 0.38), and 1.17 ± 0.59 (0.62 ± 0.39) gC m^{-2} day^{-1} respectively when using the 10 pristine sites only. This indicates that improving the vegetation description of the ORCHIDEE-PEAT improved the model's performance in simulating CO_2 fluxes of peatlands. Moreover, for simulations at the European scale using ORCHIDEE-PEAT v.3.0, multi-site optimized parameters from this study may be a suitable approach, especially in the region with little disturbance.

From the single-site calibration, we found trait (parameters)-climate relationships (Figure 7, Figures S5-S8 in Supporting Information S1). However, only 10 important parameters were calibrated in this study. Considering that ORCHIDEE includes a significantly larger number of parameters, it would be worthwhile to test the optimization of more parameters and consider more sites in the future to further explore trait-climate relationships and underlying mechanisms. Additionally, among the 14 peatlands used in this study, 13 are fens and only 1 is bog.

Bogs rely primarily on precipitation for water supply, making them nutrient-poor (ombrotrophic) and highly acidic, whereas fens are fed by groundwater or surface runoff, which provides mineral-rich water, making them nutrient-rich (minerotrophic) and typically neutral to slightly alkaline pH (Golovchenko et al., 2007; Keller et al., 2006). These differences significantly influence plant communities and ecological characteristics (Aerts et al., 1999; Pedrotti et al., 2014; Weltzin et al., 2000). Therefore, the predominance of fens in this study may limit the representativeness of the calibration for bogs, which needs to be further implemented in future work.

Compared with the standard single-site calibration (S2), our single-site calibration with prescribed WTD from field observations (S3) shows slightly improved performance (Figure 5 and Table S3 in Supporting Information S1). Prescribing WTD also led to differences in optimized parameter values (Tables S5 and S6 in Supporting Information S1), particularly $\mathbf{Q_{10}}$, defining the temperature sensitivity of SOC decomposition. The mean values of optimized $\mathbf{Q_{10}}$ across the 9 sites are 3.82 ± 1.92 and 1.76 ± 0.53 for prognostic WTD and for prescribed WTD, respectively (Table S7 in Supporting Information S1). Furthermore, although a detailed site-specific calibration of soil hydro-physical parameters was not performed, because no site data on soil porosity, compaction, and lateral water influx, was available except for water table, we acknowledge the fact that the long term WTD can be similar between sites with different porosities although its seasonal and interannual fluctuations could differ, so that prescribing the WTD in simulations correct implicitly for unresolved soil hydrological parameters differences between sites.

5. Conclusion

This study developed a new version of the ORCHIDEE-PEAT model (v.3.0) by incorporating three new peatland-specific PFTs, namely deciduous broadleaf shrub, moss and lichen, as well as evergreen needleleaf tree in addition to previously peatland graminoid PFT. Simulated GPP and NEE have been evaluated at 14 European peat sites. The parameters involved in photosynthesis, autotrophic respiration, and carbon decomposition for graminoids, shrubs, and mosses and lichens, as well as stomatal conductance-related parameters for mosses and lichens, were calibrated individually for each site (single-site calibration) and across all sites (multi-site calibration). The results showed that the single-site calibration exhibited notable agreement with field observations, with a gradient pattern in calibrated parameter values primarily attributed to latitudinal differences. In comparison, multi-site calibration yielded limited improvements compared with the simulation with default parameters due to the neglect of trait-climate correlations in the model. This study is a step forward in providing a more accurate representation of peatland vegetation cover in ORCHIDEE-PEAT. Future developments should include more peatland-specific PFTs, such as boreal evergreen trees, tropical evergreen trees, and tropical raingreen trees. Additionally, incorporating trait-climate correlations into the model is warranted to enhance the reliability of quantifying peatland feedback to climate change, thereby improving the accuracy of global projections concerning the effects of peatland vegetation changes on the carbon cycle.

Acknowledgments

The authors want to thank the editors, as well as two anonymous reviewers for their valuable and constructive comments that have improved the manuscript. This study was supported by Horizon Europe Grant Wet Horizons (GAP-101056848). C. Q. acknowledges the financial support from the National Key R&D Program of China (2022YFF0802104). E. L. -B. and E. S. consider this study a contribution to GreenFeedBack (Greenhouse gas fluxes and earth system feedbacks) funded by the European Union's HORIZON research and innovation program under grant agreement No 101056921. J. D. is funded by the project of the Ministry of Education, Youth and Sports of the Czech Republic LM2023048. DE-Zrk is operated as part of the Terrestrial Environmental Observatories Network (TERENO) of the Helmholtz Association of German Research Centers. The installation, data collection and analysis of the EC flux tower of FR-LGt peatland are supported by the Labex VOLTAIRE (ANR-10-LABX-100-01) and funded as part of the CAREX project supported by the Loire Valley Center Region and the FEDER, in the framework of the French Peatland Observatory, SNO-Tourbières, accredited by CNRS-INSU. We would like to thank S. Chevrier, G. Challumeau, A. Jacotot, and S. Gogo for their help with the installation, maintenance, data collection and analysis of the EC flux tower of FR-LGt peatland. We thank ICOS for providing the meteorological and CO_2 flux data from the DK-Skj and SE-Deg sites, and FLUXNET for providing the meteorological and CO_2 flux data from the DE-Akm site.

Data Availability Statement

The ORCHIDEE-PEAT model (Liu, 2024) used in this study is open-source and distributed under the CeCILL (CEA CNRS INRIA Logiciel Libre) license. It is deposited at https://forge.ipsl.jussieu.fr/orchidee/wiki/Group-Activities/CodeAvalaibilityPublication/ORCHIDEE-PEAT_V3. Alternatively, the model, alongside the field data used in this study including meteorological forcing, field observed CO_2 fluxes and WTD, and the ORCHIDEE data assimilation system (ORCHIDAS), is accessible (Liu, 2025) via Zenodo at: https://doi.org/10.5281/zenodo.14605345.

References

Aerts, R. (2006). The freezer defrosting: Global warming and litter decomposition rates in cold biomes. *Journal of Ecology*, *94*(4), 713–724. https://doi.org/10.1111/j.1365-2745.2006.01142.x

Aerts, R., Verhoeven, J. T. A., & Whigham, D. F. (1999). Plant-mediated controls on nutrient cycling in temperate fens and bogs. *Ecology*, *80*(7), 2170–2181. https://doi.org/10.1890/0012-9658(1999)080[2170:PMCONC]2.0.CO;2

Ågren, G. I., & Wetterstedt, J. Å. M. (2007). What determines the temperature response of soil organic matter decomposition? *Soil Biology and Biochemistry*, *39*(7), 1794–1798. https://doi.org/10.1016/j.soilbio.2007.02.007

Ahmad, S., Liu, H., Günther, A., Couwenberg, J., & Lennartz, B. (2020). Long-term rewetting of degraded peatlands restores hydrological buffer function. *Science of The Total Environment*, *749*, 141571. https://doi.org/10.1016/j.scitotenv.2020.141571

Akaike, H. (1974). A new look at the statistical model identification. *IEEE Trans. Autom. Control*, *19*(6), 716–723. https://doi.org/10.1109/TAC.1974.1100705

Aro, E.-M., & Gerbaud, A. (1984). Photosynthesis and photorespiration in mosses. In C. Sybesma (Ed.), *Advances in Photosynthesis Research: Proceedings of the VIth International Congress on Photosynthesis, Brussels, Belgium, August 1–6, 1983 Volume 3* (pp. 867–870). Springer. https://doi.org/10.1007/978-94-017-4973-2_198

Artz, R. R. E., Coyle, M., Donaldson-Selby, G., & Morrison, R. (2022). Net carbon dioxide emissions from an eroding Atlantic blanket bog. *Biogeochemistry*, *159*(2), 233–250. https://doi.org/10.1007/s10533-022-00923-x

Atkin, O. K., Bloomfield, K. J., Reich, P. B., Tjoelker, M. G., Asner, G. P., Bonal, D., et al. (2015). Global variability in leaf respiration in relation to climate, plant functional types and leaf traits. *New Phytologist*, *206*(2), 614–636. https://doi.org/10.1111/nph.13253

Atkin, O. K., & Tjoelker, M. G. (2003). Thermal acclimation and the dynamic response of plant respiration to temperature. *Trends in Plant Science*, *8*(7), 343–351. https://doi.org/10.1016/S1360-1385(03)00136-5

Aurela, M., Lohila, A., Tuovinen, J.-P., Hatakka, J., Penttilä, T., & Laurila, T. (2015). Carbon dioxide and energy flux measurements in four northern-boreal ecosystems at Pallas 20.

Aurela, M., Riutta, T., Laurila, T., Tuovinen, J.-P., Vesala, T., Tuittila, E.-S., et al. (2007). CO2 exchange of a sedge fen in southern Finland—The impact of a drought period. *Tellus B: Chemical and Physical Meteorology*, *59*(5), 826. https://doi.org/10.1111/j.1600-0889.2007.00309.x

Bacour, C., MacBean, N., Chevallier, F., Léonard, S., Koffi, E. N., & Peylin, P. (2023). Assimilation of multiple datasets results in large differences in regional-to global-scale NEE and GPP budgets simulated by a terrestrial biosphere model. *Biogeosciences*, *20*(6), 1089–1111. https://doi.org/10.5194/bg-20-1089-2023

Ball, J. T., Woodrow, I. E., & Berry, J. A. (1987). A model predicting stomatal conductance and its contribution to the control of photosynthesis under different environmental conditions. In J. Biggins (Ed.), *Progress in photosynthesis Research: Volume 4 Proceedings of the VIIth International Congress on Photosynthesis Providence, Rhode Island, USA, August 10–15, 1986* (pp. 221–224). Springer. https://doi.org/10.1007/978-94-017-0519-6_48

Banks, H. T., & Joyner, M. L. (2017). AIC under the framework of least squares estimation. *Applied Mathematics Letters*, *74*, 33–45. https://doi.org/10.1016/j.aml.2017.05.005

Bastrikov, V., MacBean, N., Bacour, C., Santaren, D., Kuppel, S., & Peylin, P. (2018). Land surface model parameter optimisation using in situ flux data: Comparison of gradient-based versus random search algorithms (a case study using ORCHIDEE v1.9.5.2). *Geoscientific Model Development*, *11*(12), 4739–4754. https://doi.org/10.5194/gmd-11-4739-2018

Bazzi, H., Ciais, P., Abbessi, E., Makowski, D., Santaren, D., Ceschia, E., et al. (2024). Assimilating Sentinel-2 data in a modified vegetation photosynthesis and respiration model (VPRM) to improve the simulation of croplands CO2 fluxes in Europe. *International Journal of Applied Earth Observation and Geoinformation*, *127*, 103666. https://doi.org/10.1016/j.jag.2024.103666

Bernhofer, C., Grünwald, T., Moderow, U., Hehn, M., Eichelmann, U., Prasse, H., & Postel, U. (2016). FLUXNET2015 DE-Akm Anklam. In *FluxNet*. TU Dresden.

Bhuiyan, R., Minkkinen, K., Helmisaari, H.-S., Ojanen, P., Penttilä, T., & Laiho, R. (2017). Estimating fine-root production by tree species and understorey functional groups in two contrasting peatland forests. *Plant and Soil*, *412*(1), 299–316. https://doi.org/10.1007/s11104-016-3070-3

Bona, K. A., Shaw, C., Thompson, D. K., Hararuk, O., Webster, K., Zhang, G., et al. (2020). The Canadian model for peatlands (CaMP): A peatland carbon model for national greenhouse gas reporting. *Ecological Modelling*, *431*, 109164. https://doi.org/10.1016/j.ecolmodel.2020.109164

Booth, R. K., Hotchkiss, S. C., & Wilcox, D. A. (2005). Discoloration of polyvinyl chloride (PVC) tape as a proxy for water-table depth in peatlands: Validation and assessment of seasonal variability. *Functional Ecology*, *19*(6), 1040–1047. https://doi.org/10.1111/j.1365-2435.2005.01048.x

Bradford, M. A., Davies, C. A., Frey, S. D., Maddox, T. R., Melillo, J. M., Mohan, J. E., et al. (2008). Thermal adaptation of soil microbial respiration to elevated temperature. *Ecology Letters*, *11*(12), 1316–1327. https://doi.org/10.1111/j.1461-0248.2008.01251.x

Bruhl, J., & Wilson, K. (2007). Towards a Comprehensive survey of C3 and C4 photosynthetic pathways in cyperaceae. *Aliso: A Journal of Systematic and Floristic Botany*, *23*(1), 99–148. https://doi.org/10.5642/aliso.20072301.11

Byun, E., Rezanezhad, F., Fairbairn, L., Slowinski, S., Basiliko, N., Price, J. S., et al. (2021). Temperature, moisture and freeze–thaw controls on CO2 production in soil incubations from northern peatlands. *Scientific Reports*, *11*(1), 23219. https://doi.org/10.1038/s41598-021-02606-3

Chadburn, S. E., Burke, E. J., Gallego-Sala, A. V., Smith, N. D., Bret-Harte, M. S., Charman, D. J., et al. (2022). A new approach to simulate peat accumulation, degradation and stability in a global land surface scheme (JULES vn5.8_accumulate_soil) for northern and temperate peatlands. *Geoscientific Model Development*, *15*(4), 1633–1657. https://doi.org/10.5194/gmd-15-1633-2022

Chater, C., Gray, J. E., & Beerling, D. J. (2013). Early evolutionary acquisition of stomatal control and development gene signalling networks. *Curr. Opin. Plant Biol., Cell Signalling and Gene Regulation*, *16*(5), 638–646. https://doi.org/10.1016/j.pbi.2013.06.013

Chaudhary, N., Miller, P. A., & Smith, B. (2017). Modelling Holocene peatland dynamics with an individual-based dynamic vegetation model. *Biogeosciences*, *14*(10), 2571–2596. https://doi.org/10.5194/bg-14-2571-2017

Chen, H., Xu, X., Fang, C., Li, B., & Nie, M. (2021). Differences in the temperature dependence of wetland CO2 and CH4 emissions vary with water table depth. *Nature Climate Change*, *11*(9), 766–771. https://doi.org/10.1038/s41558-021-01108-4

Chen, H., Zou, J., Cui, J., Nie, M., & Fang, C. (2018). Wetland drying increases the temperature sensitivity of soil respiration. *Soil Biology and Biochemistry*, *120*, 24–27. https://doi.org/10.1016/j.soilbio.2018.01.035

Cook, B. I., Smerdon, J. E., Seager, R., & Coats, S. (2014). Global warming and 21st century drying. *Climate Dynamics*, *43*(9), 2607–2627. https://doi.org/10.1007/s00382-014-2075-y

Cornelissen, J. H. C., Van Bodegom, P. M., Aerts, R., Callaghan, T. V., Van Logtestijn, R. S. P., Alatalo, J., et al. (2007). Global negative vegetation feedback to climate warming responses of leaf litter decomposition rates in cold biomes. *Ecology Letters*, *10*(7), 619–627. https://doi.org/10.1111/j.1461-0248.2007.01051.x

D'Angelo, B., Leroy, F., Guimbaud, C., Jacotot, A., Zocatelli, R., Gogo, S., & Laggoun-Défarge, F. (2021). Carbon balance and spatial variability of CO2 and CH4 fluxes in a sphagnum-dominated peatland in a temperate climate. *Wetlands (Wilmington, N. C.)*, *41*(1), 5. https://doi.org/10.1007/s13157-021-01411-y

Davidson, E. A., & Janssens, I. A. (2006). Temperature sensitivity of soil carbon decomposition and feedbacks to climate change. *Nature*, *440*(7081), 165–173. https://doi.org/10.1038/nature04514

Dawson, Q. L. (2006). Low-lying agricultural peatland sustainability under managed water regimes.

Dimitrov, D. D., Grant, R. F., Lafleur, P. M., & Humphreys, E. R. (2011). Modeling the effects of hydrology on gross primary productivity and net ecosystem productivity at Mer Bleue bog. *Journal of Geophysical Research*, *116*(G4), G04010. https://doi.org/10.1029/2010JG001586

Dorrepaal, E. (2007). Are plant growth-form-based classifications useful in predicting northern ecosystem carbon cycling feedbacks to climate change? *Journal of Ecology*, *95*(6), 1167–1180. https://doi.org/10.1111/j.1365-2745.2007.01294.x

Druel, A., Peylin, P., Krinner, G., Ciais, P., Viovy, N., Peregon, A., et al. (2017). Towards a more detailed representation of high-latitude vegetation in the global land surface model ORCHIDEE (ORC-HL-VEGv1.0). *Geoscientific Model Development*, *10*(12), 4693–4722. https://doi.org/10.5194/gmd-10-4693-2017

Evans, C. D., Peacock, M., Baird, A. J., Artz, R. R. E., Burden, A., Callaghan, N., et al. (2021). Overriding water table control on managed peatland greenhouse gas emissions. *Nature*, *593*(7860), 548–552. https://doi.org/10.1038/s41586-021-03523-1

Evans, J. R. (1989). Photosynthesis and nitrogen relationships in leaves of C3 plants. *Oecologia*, *78*(1), 9–19. https://doi.org/10.1007/BF00377192

Fairbairn, L., Rezanezhad, F., Gharasoo, M., Parsons, C. T., Macrae, M. L., Slowinski, S., & Van Cappellen, P. (2023). Relationship between soil CO2 fluxes and soil moisture: Anaerobic sources explain fluxes at high water content. *Geoderma (Amsterdam)*, *434*, 116493. https://doi.org/10.1016/j.geoderma.2023.116493

Fang, C., Smith, P., Moncrieff, J. B., & Smith, J. U. (2005). Similar response of labile and resistant soil organic matter pools to changes in temperature. *Nature*, *433*(7021), 57–59. https://doi.org/10.1038/nature03138

Fang, J., Piao, S., Field, C. B., Pan, Y., Guo, Q., Zhou, L., et al. (2003). Increasing net primary production in China from 1982 to 1999. *Frontiers in Ecology and the Environment*, *1*(6), 293–297. https://doi.org/10.1890/1540-9295(2003)001[0294:INPPIC]2.0.CO;2

Farquhar, G. D., von Caemmerer, S., & Berry, J. A. (1980). A biochemical model of photosynthetic CO2 assimilation in leaves of C3 species. *Planta*, *149*(1), 78–90. https://doi.org/10.1007/BF00386231

Franz, D., Koebsch, F., Larmanou, E., Augustin, J., & Sachs, T. (2016). High net CO2 and CH4 release at a eutrophic shallow lake on a formerly drained fen. *Biogeosciences*, *13*(10), 3051–3070. https://doi.org/10.5194/bg-13-3051-2016

Frolking, S., & Roulet, N. T. (2007). Holocene radiative forcing impact of northern peatland carbon accumulation and methane emissions. *Global Change Biology*, *13*(5), 1079–1088. https://doi.org/10.1111/j.1365-2486.2007.01339.x

Frolking, S., Roulet, N. T., Tuittila, E., Bubier, J. L., Quillet, A., Talbot, J., & Richard, P. J. H. (2010). A new model of Holocene peatland net primary production, decomposition, water balance, and peat accumulation. *Earth System Dynamics*, *1*(1), 1–21. https://doi.org/10.5194/esd-1-1-2010

Frolking, S., Talbot, J., Jones, M. C., Treat, C. C., Kauffman, J. B., Tuittila, E.-S., & Roulet, N. (2011). Peatlands in the Earth's 21st century climate system. *Environmental Reviews*, *19*(NA), 371–396. https://doi.org/10.1139/a11-014

Gleckler, P. J., Taylor, K. E., & Doutriaux, C. (2008). Performance metrics for climate models. *Journal of Geophysical Research*, *113*(D6), D06104. https://doi.org/10.1029/2007JD008972

Gogo, S., Laggoun-Défarge, F., Merzouki, F., Mounier, S., Guirimand-Dufour, A., Jozja, N., et al. (2016). In situ and laboratory non-additive litter mixture effect on C dynamics of Sphagnum rubellum and Molinia caerulea litters. *Journal of Soils and Sediments*, *16*(1), 13–27. https://doi.org/10.1007/s11368-015-1178-3

Goldberg, D. (1989). Genetic algorithms. In *Search, Optimization and Ma- chine Learning*. Addison-Wesley.432.

Golovchenko, A. V., Tikhonova, E. Y., & Zvyagintsev, D. G. (2007). Abundance, biomass, structure, and activity of the microbial complexes of minerotrophic and ombrotrophic peatlands. *Microbiology*, *76*(5), 630–637. https://doi.org/10.1134/S0026261707050177

Górecki, K., Rastogi, A., Stróżecki, M., Gąbka, M., Lamentowicz, M., Łuców, D., et al. (2021). Water table depth, experimental warming, and reduced precipitation impact on litter decomposition in a temperate *Sphagnum*-peatland. *Science of The Total Environment*, *771*, 145452. https://doi.org/10.1016/j.scitotenv.2021.145452

Gorham, E. (1991). Northern peatlands: Role in the carbon cycle and probable responses to climatic warming. *Ecological Applications*, *1*(2), 182–195. https://doi.org/10.2307/1941811

Grosse, G., Harden, J., Turetsky, M., McGuire, A. D., Camill, P., Tarnocai, C., et al. (2011). Vulnerability of high-latitude soil organic carbon in North America to disturbance. *Journal of Geophysical Research*, *116*(G4), G00K06. https://doi.org/10.1029/2010JG001507

Guimberteau, M., Zhu, D., Maignan, F., Huang, Y., Yue, C., Dantec-Nédélec, S., et al. (2018). ORCHIDEE-MICT (v8.4.1), a land surface model for the high latitudes: Model description and validation. *Geoscientific Model Development*, *11*(1), 121–163. https://doi.org/10.5194/gmd-11-121-2018

Haig, D. (2013). Filial mistletoes: The functional morphology of moss sporophytes. *Annals of Botany*, *111*(3), 337–345. https://doi.org/10.1093/aob/mcs295

Hardie, S. M. L., Garnett, M. H., Fallick, A. E., Rowland, A. P., Ostle, N. J., & Flowers, T. H. (2011). Abiotic drivers and their interactive effect on the flux and carbon isotope (14C and δ13C) composition of peat-respired CO2. *Soil Biology and Biochemistry*, *43*(12), 2432–2440. https://doi.org/10.1016/j.soilbio.2011.08.010

Harris, I. C. (2023). Cru JRA v2.4: A forcings dataset of gridded land surface blend of climatic research unit (CRU) and Japanese reanalysis (JRA) data; January 1901–December 2022. NERC EDS Centre for Environmental Data Analysis, dd,mm,yyyy.

Hartig, F., Dyke, J., Hickler, T., Higgins, S. I., O'Hara, R. B., Scheiter, S., & Huth, A. (2012). Connecting dynamic vegetation models to data – An inverse perspective. *Journal of Biogeography*, *39*(12), 2240–2252. https://doi.org/10.1111/j.1365-2699.2012.02745.x

Hartley, I. P., Hopkins, D. W., Garnett, M. H., Sommerkorn, M., & Wookey, P. A. (2009). No evidence for compensatory thermal adaptation of soil microbial respiration in the study of Bradford et al. (2008). *Ecology Letters*, *12*(7), E12–E14. https://doi.org/10.1111/j.1461-0248.2009.01300.x

Haupt, R. L., & Haupt, S. E. (2004). *Practical genetic Algorithms*. John Wiley and Sons, Inc. https://doi.org/10.1002/0471671746

Helbig, M., Waddington, J. M., Alekseychik, P., Amiro, B. D., Aurela, M., Barr, A. G., et al. (2020). Increasing contribution of peatlands to boreal evapotranspiration in a warming climate. *Nature Climate Change*, *10*(6), 555–560. https://doi.org/10.1038/s41558-020-0763-7

Herbst, M., Friborg, T., Ringgaard, R., & Soegaard, H. (2011). Interpreting the variations in atmospheric methane fluxes observed above a restored wetland. *Agricultural and Forest Meteorology*, *151*(7), 841–853. https://doi.org/10.1016/j.agrformet.2011.02.002

Hilasvuori, E., Akujärvi, A., Fritze, H., Karhu, K., Laiho, R., Mäkiranta, P., et al. (2013). Temperature sensitivity of decomposition in a peat profile. *Soil Biology and Biochemistry*, *67*, 47–54. https://doi.org/10.1016/j.soilbio.2013.08.009

Ise, T., Dunn, A. L., Wofsy, S. C., & Moorcroft, P. R. (2008). High sensitivity of peat decomposition to climate change through water-table feedback. *Nature Geoscience*, *1*(11), 763–766. https://doi.org/10.1038/ngeo331

Ise, T., & Moorcroft, P. R. (2006). The global-scale temperature and moisture dependencies of soil organic carbon decomposition: An analysis using a mechanistic decomposition model. *Biogeochemistry*, *80*(3), 217–231. https://doi.org/10.1007/s10533-006-9019-5

Jarvis, P. G. (1995). Scaling processes and problems. *Plant, Cell and Environment*, *18*(10), 1079–1089. https://doi.org/10.1111/j.1365-3040.1995.tb00620.x

Juszczak, R., Humphreys, E., Acosta, M., Michalak-Galczewska, M., Kayzer, D., & Olejnik, J. (2013). Ecosystem respiration in a heterogeneous temperate peatland and its sensitivity to peat temperature and water table depth. *Plant and Soil*, *366*(1–2), 505–520. https://doi.org/10.1007/s11104-012-1441-y

Kalhori, A., Wille, C., Gottschalk, P., Li, Z., Hashemi, J., Kemper, K., & Sachs, T. (2024). Temporally dynamic carbon dioxide and methane emission factors for rewetted peatlands. *Communications Earth & Environment*, *5*, 1–11. https://doi.org/10.1038/s43247-024-01226-9

Kattge, J., Knorr, W., Raddatz, T., & Wirth, C. (2009). Quantifying photosynthetic capacity and its relationship to leaf nitrogen content for global-scale terrestrial biosphere models. *Global Change Biology*, *15*(4), 976–991. https://doi.org/10.1111/j.1365-2486.2008.01744.x

Keller, J. K., Bauers, A. K., Bridgham, S. D., Kellogg, L. E., & Iversen, C. M. (2006). Nutrient control of microbial carbon cycling along an ombrotrophic-minerotrophic peatland gradient. *Journal of Geophysical Research*, *111*(G3), G03006. https://doi.org/10.1029/2005JG000152

Koven, C. D., Hugelius, G., Lawrence, D. M., & Wieder, W. R. (2017). Higher climatological temperature sensitivity of soil carbon in cold than warm climates. *Nature Climate Change*, *7*(11), 817–822. https://doi.org/10.1038/nclimate3421

Koven, C. D., Ringeval, B., Friedlingstein, P., Ciais, P., Cadule, P., Khvorostyanov, D., et al. (2011). Permafrost carbon-climate feedbacks accelerate global warming. *Proceedings of the National Academy of Sciences*, *108*(36), 14769–14774. https://doi.org/10.1073/pnas.1103910108

Krinner, G., Viovy, N., De Noblet-Ducoudré, N., Ogée, J., Polcher, J., Friedlingstein, P., et al. (2005). A dynamic global vegetation model for studies of the coupled atmosphere-biosphere system: Dvgm for coupled climate studies. *Global Biogeochemical Cycles*, *19*(1), GB1015. https://doi.org/10.1029/2003GB002199

Kroner, Y., & Way, D. A. (2016). Carbon fluxes acclimate more strongly to elevated growth temperatures than to elevated CO2 concentrations in a northern conifer. *Global Change Biology*, *22*(8), 2913–2928. https://doi.org/10.1111/gcb.13215

Kuiper, J. J., Mooij, W. M., Bragazza, L., & Robroek, B. J. M. (2014). Plant functional types define magnitude of drought response in peatland CO2 exchange. *Ecology*, *95*(1), 123–131. https://doi.org/10.1890/13-0270.1

Kuppel, S., Peylin, P., Maignan, F., Chevallier, F., Kiely, G., Montagnani, L., & Cescatti, A. (2014). Model–data fusion across ecosystems: From multisite optimizations to global simulations. *Geoscientific Model Development*, *7*(6), 2581–2597. https://doi.org/10.5194/gmd-7-2581-2014

Kwon, M. J., Ballantyne, A., Ciais, P., Qiu, C., Salmon, E., Raoult, N., et al. (2022). Lowering water table reduces carbon sink strength and carbon stocks in northern peatlands. *Global Change Biology*, *28*(22), 6752–6770. https://doi.org/10.1111/gcb.16394

Lafleur, P. M., Moore, T. R., Roulet, N. T., & Frolking, S. (2005). Ecosystem respiration in a cool temperate bog depends on peat temperature but not water table. *Ecosystems (New York)*, *8*(6), 619–629. https://doi.org/10.1007/s10021-003-0131-2

Laine, A. M., Korrensalo, A., & Tuittila, E.-S. (2022). Plant functional traits play the second fiddle to plant functional types in explaining peatland CO2 and CH4 gas exchange. *The Science of the Total Environment*, *834*, 155352. https://doi.org/10.1016/j.scitotenv.2022.155352

Laine, A. M., Mehtätalo, L., Tolvanen, A., Frolking, S., & Tuittila, E.-S. (2019). Impacts of drainage, restoration and warming on boreal wetland greenhouse gas fluxes. *Science of The Total Environment*, *647*, 169–181. https://doi.org/10.1016/j.scitotenv.2018.07.390

Largeron, C., Krinner, G., Ciais, P., & Brutel-Vuilmet, C. (2017). Implementing northern peatlands in a global land surface model:description and evaluation in the ORCHIDEE high latitude versionmodel. *ORC-HL-PEAT)*. https://doi.org/10.5194/gmd-2017-141

Lasslop, G., Reichstein, M., Kattge, J., & Papale, D. (2008). Influences of observation errors in eddy flux data on inverse model parameter estimation. *Biogeosciences*, *5*, 1311–1324. https://doi.org/10.5194/bg-5-1311-2008

Leifeld, J., & Menichetti, L. (2018). The underappreciated potential of peatlands in global climate change mitigation strategies. *Nature Communications*, *9*(1), 1071. https://doi.org/10.1038/s41467-018-03406-6

Leifeld, J., Wüst-Galley, C., & Page, S. (2019). Intact and managed peatland soils as a source and sink of GHGs from 1850 to 2100. *Nature Climate Change*, *9*, 945–947. https://doi.org/10.1038/s41558-019-0615-5

Leppä, K., Korkiakoski, M., Nieminen, M., Laiho, R., Hotanen, J.-P., Kieloaho, A.-J., et al. (2020). Vegetation controls of water and energy balance of a drained peatland forest: Responses to alternative harvesting practices. *Agricultural and Forest Meteorology*, *295*, 108198. https://doi.org/10.1016/j.agrformet.2020.108198

Letts, M. G., Roulet, N. T., Comer, N. T., Skarupa, M. R., & Verseghy, D. L. (2000). Parametrization of peatland hydraulic properties for the Canadian land surface scheme. *Atmosphere-Ocean*, *38*(1), 141–160. https://doi.org/10.1080/07055900.2000.9649643

Leuning, R. (2002). Temperature dependence of two parameters in a photosynthesis model. *Plant, Cell and Environment*, *25*(9), 1205–1210. https://doi.org/10.1046/j.1365-3040.2002.00898.x

Li, J., Nie, M., Pendall, E., Reich, P. B., Pei, J., Noh, N. J., et al. (2020). Biogeographic variation in temperature sensitivity of decomposition in forest soils. *Global Change Biology*, *26*(3), 1873–1885. https://doi.org/10.1111/gcb.14838

Li, J., Pei, J., Pendall, E., Fang, C., & Nie, M. (2020). Spatial heterogeneity of temperature sensitivity of soil respiration: A global analysis of field observations. *Soil Biology and Biochemistry*, *141*, 107675. https://doi.org/10.1016/j.soilbio.2019.107675

Liu, H., Rezanezhad, F., Zhao, Y., He, H., Van Cappellen, P., & Lennartz, B. (2024). The apparent temperature sensitivity (Q10) of peat soil respiration: A synthesis study. *Geoderma (Amsterdam)*, *443*, 116844. https://doi.org/10.1016/j.geoderma.2024.116844

Liu, L. (2024). ORCHIDEE-PEAT_V3 [Software]. *ORCHIDEE-Wiki*. https://forge.ipsl.jussieu.fr/orchidee/wiki/GroupActivities/CodeAvalaibilityPublication/ORCHIDEE-PEAT_V3

Liu, L. (2025). Field data and code for JAMES paper: Assessing CO_2 fluxes for European peatlands in ORCHIDEE-PEAT with multiple plant functional types [Dataset]. *Zenodo*. https://doi.org/10.5281/zenodo.14605345

Liu, L., Gudmundsson, L., Hauser, M., Qin, D., Li, S., & Seneviratne, S. I. (2020). Soil moisture dominates dryness stress on ecosystem production globally. *Nature Communications*, *11*(1), 4892. https://doi.org/10.1038/s41467-020-18631-1

Loisel, J., Gallego-Sala, A. V., Amesbury, M. J., Magnan, G., Anshari, G., Beilman, D. W., et al. (2021). Expert assessment of future vulnerability of the global peatland carbon sink. *Nature Climate Change*, *11*(1), 70–77. https://doi.org/10.1038/s41558-020-00944-0

López-Blanco, E., Lund, M., Williams, M., Tamstorf, M. P., Westergaard-Nielsen, A., Exbrayat, J.-F., et al. (2017a). Exchange of CO2 in Arctic tundra: Impacts of meteorological variations and biological disturbance. *Biogeosciences*, *14*(19), 4467–4483. https://doi.org/10.5194/bg-14-4467-2017

Ma, S., Jiang, L., Wilson, R. M., Chanton, J., Niu, S., Iversen, C. M., et al. (2023). Thermal acclimation of plant photosynthesis and autotrophic respiration in a northern peatland. *Environmental Research: Climate*, *2*, 025003. https://doi.org/10.1088/2752-5295/acc67e

MacDonald, G. M., Beilman, D. W., Kremenetski, K. V., Sheng, Y., Smith, L. C., & Velichko, A. A. (2006). Rapid early development of circumarctic peatlands and atmospheric CH 4 and CO 2 variations. *Science*, *314*(5797), 285–288. https://doi.org/10.1126/science.1131722

Mahmud, K., Scott, R. L., Biederman, J. A., Litvak, M. E., Kolb, T., Meyers, T. P., et al. (2021). Optimizing carbon cycle parameters drastically improves terrestrial biosphere model underestimates of dryland mean net CO2 flux and its inter-annual variability. *Journal of Geophysical Research: Biogeosciences*, *126*(10), e2021JG006400. https://doi.org/10.1029/2021JG006400

Maire, V., Wright, I. J., Prentice, I. C., Batjes, N. H., Bhaskar, R., van Bodegom, P. M., et al. (2015). Global effects of soil and climate on leaf photosynthetic traits and rates. *Global Ecology and Biogeography*, *24*(6), 706–717. https://doi.org/10.1111/geb.12296

Mejdová, M., Dušek, J., Foltýnová, L., Macálková, L., & Čížková, H. (2021). Photosynthetic parameters of a sedge-grass marsh as a big-leaf: Effect of plant species composition. *Scientific Reports*, *11*(1), 3723. https://doi.org/10.1038/s41598-021-82382-2

Menberu, M. W., Tahvanainen, T., Marttila, H., Irannezhad, M., Ronkanen, A.-K., Penttinen, J., & Kløve, B. (2016). Water-table-dependent hydrological changes following peatland forestry drainage and restoration: Analysis of restoration success. *Water Resources Research*, *52*(5), 3742–3760. https://doi.org/10.1002/2015WR018578

Mikaloff Fletcher, S. E., Tans, P. P., Bruhwiler, L. M., Miller, J. B., & Heimann, M. (2004). CH4 sources estimated from atmospheric observations of CH4 and its 13C/12C isotopic ratios: 2. Inverse modeling of CH4 fluxes from geographical regions. *Global Biogeochemical Cycles*, *18*(4), GB4004. https://doi.org/10.1029/2004GB002224

Minasny, B., Berglund, Ö., Connolly, J., Hedley, C., de Vries, F., Gimona, A., et al. (2019). Digital mapping of peatlands – a critical review. *Earth-Science Reviews*, *196*, 102870. https://doi.org/10.1016/j.earscirev.2019.05.014

Morris, P. J., Waddington, J. M., Benscoter, B. W., & Turetsky, M. R. (2011). Conceptual frameworks in peatland ecohydrology: Looking beyond the two-layered (acrotelm–catotelm) model. *Ecohydrology*, *4*(1), 1–11. https://doi.org/10.1002/eco.191

Moyano, F. E., Vasilyeva, N., Bouckaert, L., Cook, F., Craine, J., Curiel Yuste, J., et al. (2012). The moisture response of soil heterotrophic respiration: Interaction with soil properties. *Biogeosciences*, *9*(3), 1173–1182. https://doi.org/10.5194/bg-9-1173-2012

Mozafari, B., Bruen, M., Donohue, S., Renou-Wilson, F., & O'Loughlin, F. (2023). Peatland dynamics: A review of process-based models and approaches. *The Science of the Total Environment*, *877*, 162890. https://doi.org/10.1016/j.scitotenv.2023.162890

Murphy, M. T., & Moore, T. R. (2010). Linking root production to aboveground plant characteristics and water table in a temperate bog. *Plant and Soil*, *336*(1–2), 219–231. https://doi.org/10.1007/s11104-010-0468-1

Nemani, R. R., Keeling, C. D., Hashimoto, H., Jolly, W. M., Piper, S. C., Tucker, C. J., et al. (2003). Climate-driven increases in global terrestrial net primary production from 1982 to 1999. *Science*, *300*(5625), 1560–1563. https://doi.org/10.1126/science.1082750

Nijp, J. J., Limpens, J., Metselaar, K., van der Zee, S. E. A. T. M., Berendse, F., & Robroek, B. J. M. (2014). Can frequent precipitation moderate the impact of drought on peatmoss carbon uptake in northern peatlands? *New Phytologist*, *203*(1), 70–80. https://doi.org/10.1111/nph.12792

Niu, B., Zhang, X., Piao, S., Janssens, I. A., Fu, G., He, Y., et al. (2021). Warming homogenizes apparent temperature sensitivity of ecosystem respiration. *Science Advances*, *7*(15), eabc7358. https://doi.org/10.1126/sciadv.abc7358

Niu, S., Luo, Y., Fei, S., Yuan, W., Schimel, D., Law, B. E., et al. (2012). Thermal optimality of net ecosystem exchange of carbon dioxide and underlying mechanisms. *New Phytologist*, *194*(3), 775–783. https://doi.org/10.1111/j.1469-8137.2012.04095.x

Noumonvi, K. D., Ågren, A. M., Ratcliffe, J. L., Öquist, M. G., Ericson, L., Tong, C. H. M., et al. (2023a). The kulbäcksliden research infrastructure: A unique setting for northern peatland studies. *Frontiers of Earth Science*, *11*, 1194749. https://doi.org/10.3389/feart.2023.1194749

Ordoñez, J. C., van Bodegom, P. M., Witte, J.-P. M., Wright, I. J., Reich, P. B., & Aerts, R. (2009). A global study of relationships between leaf traits, climate and soil measures of nutrient fertility. *Global Ecology and Biogeography*, *18*(2), 137–149. https://doi.org/10.1111/j.1466-8238.2008.00441.x

Parish, F., Sirin, A. A., Charman, D., Joosten, H., Minaeva, T. Y., & Silvius, M., (2008). Assessment on peatlands, biodiversity and climate change.

Parton, W. J., Stewart, J. W. B., & Cole, C. V. (1988). Dynamics of C, N, P and S in grassland soils: A model. *Biogeochemistry*, *5*(1), 109–131. https://doi.org/10.1007/BF02180320

Peaucelle, M., Bacour, C., Ciais, P., Vuichard, N., Kuppel, S., Peñuelas, J., et al. (2019). Covariations between plant functional traits emerge from constraining parameterization of a terrestrial biosphere model. *Global Ecology and Biogeography*, *28*(9), 1351–1365. https://doi.org/10.1111/geb.12937

Pedrotti, E., Rydin, H., Ingmar, T., Hytteborn, H., Turunen, P., & Granath, G. (2014). Fine-scale dynamics and community stability in boreal peatlands: Revisiting a fen and a bog in Sweden after 50 years. *Ecosphere*, *5*(10), art133. https://doi.org/10.1890/ES14-00202.1

Peng, S., Piao, S., Wang, T., Sun, J., & Shen, Z. (2009). Temperature sensitivity of soil respiration in different ecosystems in China. Soil Biology and Biochemistry. *Science Goes Underground in China*, *41*(5), 1008–1014. https://doi.org/10.1016/j.soilbio.2008.10.023

Peylin, P., Bacour, C., MacBean, N., Leonard, S., Rayner, P., Kuppel, S., et al. (2016). A new stepwise carbon cycle data assimilation system using multiple data streams to constrain the simulated land surface carbon cycle. *Geoscientific Model Development*, *9*, 3321–3346. https://doi.org/10.5194/gmd-9-3321-2016

Piao, S., Friedlingstein, P., Ciais, P., Viovy, N., & Demarty, J. (2007). Growing season extension and its impact on terrestrial carbon cycle in the Northern Hemisphere over the past 2 decades. *Global Biogeochemical Cycles*, *21*(3), GB3018. https://doi.org/10.1029/2006GB002888

Porada, P., Van Stan, J. T., & Kleidon, A. (2018). Significant contribution of non-vascular vegetation to global rainfall interception. *Nature Geoscience*, *11*(8), 563–567. https://doi.org/10.1038/s41561-018-0176-7

Qiu, C., Ciais, P., Zhu, D., Guenet, B., Peng, S., Petrescu, A. M. R., et al. (2021). Large historical carbon emissions from cultivated northern peatlands. *Science Advances*, *7*(23), eabf1332. https://doi.org/10.1126/sciadv.abf1332

Qiu, C., Zhu, D., Ciais, P., Guenet, B., Krinner, G., Peng, S., et al. (2018). ORCHIDEE-PEAT (revision 4596), a model for northern peatland CO2, water, and energy fluxes on daily to annual scales. *Geoscientific Model Development*, *11*(2), 497–519. https://doi.org/10.5194/gmd-11-497-2018

Qiu, C., Zhu, D., Ciais, P., Guenet, B., & Peng, S. (2020). The role of northern peatlands in the global carbon cycle for the 21st century. *Global Ecology and Biogeography*, *29*(5), 956–973. https://doi.org/10.1111/geb.13081

Qiu, C., Zhu, D., Ciais, P., Guenet, B., Peng, S., Krinner, G., et al. (2019). Modelling northern peatland area and carbon dynamics since the Holocene with the ORCHIDEE-PEAT land surface model (SVN r5488). *Geoscientific Model Development*, *12*(7), 2961–2982. https://doi.org/10.5194/gmd-12-2961-2019

Reich, P. B., Sendall, K. M., Stefanski, A., Wei, X., Rich, R. L., & Montgomery, R. A. (2016). Boreal and temperate trees show strong acclimation of respiration to warming. *Nature*, *531*(7596), 633–636. https://doi.org/10.1038/nature17142

Reich, P. B., Wright, I. J., & Lusk, C. H. (2007). Predicting leaf physiology from simple plant and climate attributes: A global glopnet analysis. *Ecological Applications*, *17*(7), 1982–1988. https://doi.org/10.1890/06-1803.1

Reichstein, M., Falge, E., Baldocchi, D., Papale, D., Aubinet, M., Berbigier, P., et al. (2005). On the separation of net ecosystem exchange into assimilation and ecosystem respiration: Review and improved algorithm. *Global Change Biology*, *11*(9), 1424–1439. https://doi.org/10.1111/j.1365-2486.2005.001002.x

Renou-Wilson, F., Moser, G., Fallon, D., Farrell, C. A., Müller, C., & Wilson, D. (2019). Rewetting degraded peatlands for climate and biodiversity benefits: Results from two raised bogs. *Ecological Engineering*, *127*, 547–560. https://doi.org/10.1016/j.ecoleng.2018.02.014

Robroek, B. J. M., Albrecht, R. J. H., Hamard, S., Pulgarin, A., Bragazza, L., Buttler, A., & Jassey, V. E. (2016). Peatland vascular plant functional types affect dissolved organic matter chemistry. *Plant and Soil*, *407*(1–2), 135–143. https://doi.org/10.1007/s11104-015-2710-3

Robroek, B. J. M., Jassey, V. E. J., Kox, M. A. R., Berendsen, R. L., Mills, R. T. E., Cécillon, L., et al. (2015). Peatland vascular plant functional types affect methane dynamics by altering microbial community structure. *Journal of Ecology*, *103*(4), 925–934. https://doi.org/10.1111/1365-2745.12413

Robroek, B. J. M., Schouten, M. G. C., Limpens, J., Berendse, F., & Poorter, H. (2009). Interactive effects of water table and precipitation on net CO2 assimilation of three co-occurring Sphagnum mosses differing in distribution above the water table. *Global Change Biology*, *15*(3), 680–691. https://doi.org/10.1111/j.1365-2486.2008.01724.x

Ruimy, A., Kergoat, L., Field, C. B., & Saugier, B. (1996). The use of CO2 flux measurements in models of the global terrestrial carbon budget. *Global Change Biology*, *2*(3), 287–296. https://doi.org/10.1111/j.1365-2486.1996.tb00080.x

Ruszala, E. M., Beerling, D. J., Franks, P. J., Chater, C., Casson, S. A., Gray, J. E., & Hetherington, A. M. (2011). Land plants acquired active stomatal control early in their evolutionary history. *Current Biology*, *21*(12), 1030–1035. https://doi.org/10.1016/j.cub.2011.04.044

Salmon, E., Jégou, F., Guenet, B., Jourdain, L., Qiu, C., Bastrikov, V., et al. (2022). Assessing methane emissions for northern peatlands in ORCHIDEE-PEAT revision 7020. *Geoscientific Model Development*, *15*(7), 2813–2838. https://doi.org/10.5194/gmd-15-2813-2022

Santaren, D., Peylin, P., Bacour, C., Ciais, P., & Longdoz, B. (2014). Ecosystem model optimization using in situ flux observations: Benefit of Monte Carlo versus variational schemes and analyses of the year-to-year model performances. *Biogeosciences*, *11*(24), 7137–7158. https://doi.org/10.5194/bg-11-7137-2014

Scharlemann, J. P., Tanner, E. V., Hiederer, R., & Kapos, V. (2014). Global soil carbon: Understanding and managing the largest terrestrial carbon pool. *Carbon Management*, *5*(1), 81–91. https://doi.org/10.4155/cmt.13.77

Smith, L. C., MacDonald, G. M., Velichko, A. A., Beilman, D. W., Borisova, O. K., Frey, K. E., et al. (2004). Siberian peatlands a net carbon sink and global methane source since the early holocene. *Science*, *303*(5656), 353–356. https://doi.org/10.1126/science.1090553

Smith, N. G., & Dukes, J. S. (2013). Plant respiration and photosynthesis in global-scale models: Incorporating acclimation to temperature and 2. *Global Change Biology*, *19*(1), 45–63. https://doi.org/10.1111/j.1365-2486.2012.02797.x

Spahni, R., Joos, F., Stocker, B. D., Steinacher, M., & Yu, Z. C. (2013). Transient simulations of the carbon and nitrogen dynamics in northern peatlands: From the last glacial maximum to the 21st century. *Climate of the Past*, *9*(3), 1287–1308. https://doi.org/10.5194/cp-9-1287-2013

St-Hilaire, F., Wu, J., Roulet, N. T., Frolking, S., Lafleur, P. M., Humphreys, E. R., & Arora, V. (2010). McGill wetland model: Evaluation of a peatland carbon simulator developed for global assessments. *Biogeosciences*, *7*(11), 3517–3530. https://doi.org/10.5194/bg-7-3517-2010

Swindles, G. T., Morris, P. J., Mullan, D. J., Payne, R. J., Roland, T. P., Amesbury, M. J., et al. (2019). Widespread drying of European peatlands in recent centuries. *Nature Geoscience*, *12*(11), 922–928. https://doi.org/10.1038/s41561-019-0462-z

Szafranek-Nakonieczna, A., & Stêpniewska, Z. (2014). Aerobic and anaerobic respiration in profiles of polesie lubelskie peatlands. *International Agrophysics*, *28*(2), 219–229. https://doi.org/10.2478/intag-2014-0011

Takashima, T., Hikosaka, K., & Hirose, T. (2004). Photosynthesis or persistence: Nitrogen allocation in leaves of evergreen and deciduous quercus species. *Plant, Cell and Environment*, *27*(8), 1047–1054. https://doi.org/10.1111/j.1365-3040.2004.01209.x

Tarantola, A. (2005). *Inverse problem theory and methods for model parameter estimation*. SIAM.

Taylor, K. E. (2001). Summarizing multiple aspects of model performance in a single diagram. *Journal of Geophysical Research*, *106*(D7), 7183–7192. https://doi.org/10.1029/2000JD900719

Teeri, J. A. (1981). Stable carbon isotope analysis of mosses and lichens growing in xeric and moist habitats. *The Bryologist*, *84*(1), 82–84. https://doi.org/10.2307/3242982

Toet, S., Cornelissen, J. H. C., Aerts, R., Van Logtestijn, R. S. P., De Beus, M., & Stoevelaar, R. (2006). Moss responses to elevated CO2 and variation in hydrology in a temperate lowland peatland. *Plant Ecology*, *182*(1–2), 27–40. https://doi.org/10.1007/s11258-005-9029-8

Treat, C. C., Kleinen, T., Broothaerts, N., Dalton, A. S., Dommain, R., Douglas, T. A., et al. (2019). Widespread global peatland establishment and persistence over the last 130,000 y. *Proceedings of the National Academy of Sciences*, *116*(11), 4822–4827. https://doi.org/10.1073/pnas.1813305116

Turetsky, M., Wieder, K., Halsey, L., & Vitt, D. (2002). Current disturbance and the diminishing peatland carbon sink. *Geophysical Research Letters*, *29*(11), 21-1–21–4. https://doi.org/10.1029/2001GL014000

Turetsky, M. R., Bond-Lamberty, B., Euskirchen, E., Talbot, J., Frolking, S., McGuire, A. D., & Tuittila, E.-S. (2012). The resilience and functional role of moss in boreal and arctic ecosystems. *New Phytologist*, *196*(1), 49–67. https://doi.org/10.1111/j.1469-8137.2012.04254.x

Turunen, J., Tomppo, E., Tolonen, K., & Reinikainen, A. (2002). Estimating carbon accumulation rates of undrained mires in Finland–application to boreal and subarctic regions. *The Holocene*, *12*(1), 69–80. https://doi.org/10.1191/0959683602hl522rp

van Ommen Kloeke, A. E. E., Douma, J. C., Ordoñez, J. C., Reich, P. B., & van Bodegom, P. M. (2012). Global quantification of contrasting leaf life span strategies for deciduous and evergreen species in response to environmental conditions. *Global Ecology and Biogeography*, *21*, 224–235. https://doi.org/10.1111/j.1466-8238.2011.00667.x

Walker, A. P., Beckerman, A. P., Gu, L., Kattge, J., Cernusak, L. A., Domingues, T. F., et al. (2014). The relationship of leaf photosynthetic traits – Vcmax and Jmax – To leaf nitrogen, leaf phosphorus, and specific leaf area: A meta-analysis and modeling study. *Ecology and Evolution*, *4*(16), 3218–3235. https://doi.org/10.1002/ece3.1173

Walker, A. P., Quaife, T., van Bodegom, P. M., De Kauwe, M. G., Keenan, T. F., Joiner, J., et al. (2017). The impact of alternative trait-scaling hypotheses for the maximum photosynthetic carboxylation rate (Vcmax) on global gross primary production. *New Phytologist*, *215*(4), 1370–1386. https://doi.org/10.1111/nph.14623

Walker, T. N., Ward, S. E., Ostle, N. J., & Bardgett, R. D. (2015). Contrasting growth responses of dominant peatland plants to warming and vegetation composition. *Oecologia*, *178*(1), 141–151. https://doi.org/10.1007/s00442-015-3254-1

Wang, C., Yang, J., & Zhang, Q. (2006). Soil respiration in six temperate forests in China. *Global Change Biology*, *12*(11), 2103–2114. https://doi.org/10.1111/j.1365-2486.2006.01234.x

Wang, M., Liu, H., & Lennartz, B. (2021). Small-scale spatial variability of hydro-physical properties of natural and degraded peat soils. *Geoderma (Amsterdam)*, *399*, 115123. https://doi.org/10.1016/j.geoderma.2021.115123

Wania, R., Ross, I., & Prentice, I. C. (2009a). Integrating peatlands and permafrost into a dynamic global vegetation model: 1. Evaluation and sensitivity of physical land surface processes. *Global Biogeochemical Cycles*, *23*(3). https://doi.org/10.1029/2008GB003412

Wania, R., Ross, I., & Prentice, I. C. (2009b). Integrating peatlands and permafrost into a dynamic global vegetation model: 2. Evaluation and sensitivity of vegetation and carbon cycle processes. *Global Biogeochemical Cycles*, *23*(3). https://doi.org/10.1029/2008GB003413

Weltzin, J. F., Pastor, J., Harth, C., Bridgham, S. D., Updegraff, K., & Chapin, C. T. (2000). Response of bog and fen plant communities to warming and water-table manipulations. *Ecology*, *81*(12), 3464–3478. https://doi.org/10.1890/0012-9658(2000)081[3464:ROBAFP]2.0.CO;2

Williams, T. G., & Flanagan, L. B. (1996). Effect of changes in water content on photosynthesis, transpiration and discrimination against 13CO2 and C18O16O in Pleurozium and Sphagnum. *Oecologia*, *108*(1), 38–46. https://doi.org/10.1007/BF00333212

Wright, I. J., Reich, P. B., Cornelissen, J. H. C., Falster, D. S., Garnier, E., Hikosaka, K., et al. (2005). Assessing the generality of global leaf trait relationships. *New Phytologist*, *166*(2), 485–496. https://doi.org/10.1111/j.1469-8137.2005.01349.x

Wu, Y., Verseghy, D. L., & Melton, J. R. (2016). Integrating peatlands into the coupled Canadian land surface scheme (CLASS) v3.6 and the Canadian terrestrial ecosystem model (CTEM) v2.0. *Geoscientific Model Development*, *9*(8), 2639–2663. https://doi.org/10.5194/gmd-9-2639-2016

Xi, Y., Peng, S., Ciais, P., & Chen, Y. (2021). Future impacts of climate change on inland Ramsar wetlands. *Nature Climate Change*, *11*(1), 45–51. https://doi.org/10.1038/s41558-020-00942-2

Yin, X., & Struik, P. C. (2009). C3 and C4 photosynthesis models: An overview from the perspective of crop modelling. *NJAS - Wageningen Journal of Life Sciences*, *57*(1), 27–38. https://doi.org/10.1016/j.njas.2009.07.001

Yu, Z., Loisel, J., Brosseau, D. P., Beilman, D. W., & Hunt, S. J. (2010). Global peatland dynamics since the last glacial maximum. *Geophysical Research Letters*, *37*(13), L13402. https://doi.org/10.1029/2010GL043584

Yu, Z. C. (2012). Northern peatland carbon stocks and dynamics: A review. *Biogeosciences*, *9*(10), 4071–4085. https://doi.org/10.5194/bg-9-4071-2012

Zhang, Y., Li, C., Trettin, C. C., Li, H., & Sun, G. (2002). An integrated model of soil, hydrology, and vegetation for carbon dynamics in wetland ecosystems. *Global Biogeochemical Cycles*, *16*(4), 9-1–9–17. https://doi.org/10.1029/2001GB001838

Zhao, B., Zhuang, Q., & Frolking, S. (2022). Modeling carbon accumulation and permafrost dynamics of northern peatlands since the holocene. *Journal of Geophysical Research: Biogeosciences*, *127*(11), e2022JG007009. https://doi.org/10.1029/2022JG007009

Zou, J., Ziegler, A. D., Chen, D., McNicol, G., Ciais, P., Jiang, X., et al. (2022). Rewetting global wetlands effectively reduces major greenhouse gas emissions. *Nature Geoscience*, *15*(8), 627–632. https://doi.org/10.1038/s41561-022-00989-0